Pharmacologic inhibition of Hsp90 to prevent GLT-1 degradation as an effective therapy for epilepsy

Longze Sha,[1]* Xueqin Wang,[1]* Jing Li,[1] Xinze Shi,[1] Liwen Wu,[2] Yan Shen,[1] and Qi Xu[1]

[1]State Key Laboratory of Medical Molecular Biology, Institute of Basic Medical Sciences and Neuroscience Center, Chinese Academy of Medical Sciences and Peking Union Medical College, Beijing 100005, China
[2]Department of Neurology, Peking Union Medical College Hospital, Chinese Academy of Medical Sciences and Peking Union Medical College, Beijing 100730, China

The glutamate transporter GLT-1 is critical for the maintenance of low interstitial glutamate concentrations. Loss of GLT-1 is commonly observed in neurological disorders, including temporal lobe epilepsy (TLE). Despite the hypothesis that targeting the mechanisms of GLT-1 deficiency may be a novel strategy for treating drug-resistant epilepsy, the underlying molecular cascade remains largely unknown. Here, we show that Hsp90β is up-regulated in reactive astrocytes of the epileptic hippocampus in patients with TLE and mouse models of epilepsy. Inhibition of Hsp90, but not Hsp70, increased GLT-1 levels. Mechanistically, Hsp90β recruits GLT-1 to the 20S proteasome, thereby promoting GLT-1 degradation. Hsp90 inhibitor prevents GLT-1 degradation by disrupting the association between Hsp90β and GLT-1. Using a model of TLE, we demonstrated that long-term systemic administration of 17AAG dramatically suppressed spontaneous recurrent seizures and ameliorated astrogliosis. Overall, these results suggest that up-regulation of GLT-1 by inhibiting Hsp90β in reactive astrocytes may be a potential therapeutic target for the treatment of epilepsy and excitotoxicity.

INTRODUCTION

Epilepsy is one of the most common chronic neurological diseases, yet approximately one-third of affected patients do not respond to anticonvulsive drugs that target neurons (Kwan et al., 2011). Recent studies suggest that astrocytes are a potential target for the therapeutic treatment of intractable epilepsy (Héja, 2014; Robel et al., 2015). GLT-1 (EAAT2; slc1a2) is predominantly expressed in astrocytes and responsible for maintaining low extracellular glutamate concentrations (Vandenberg and Ryan, 2013). Loss of GLT-1 has been described in many neurological disorders, including amyotrophic lateral sclerosis (ALS), Alzheimer's disease (AD), and temporal lobe epilepsy (TLE; Rothstein et al., 1995; Li et al., 1997; Proper et al., 2002; Takahashi et al., 2015). Functional studies found that mice lacking GLT-1 exhibited severe spontaneous seizures (Tanaka et al., 1997). In contrast, GLT-1 transgenic mice are resistant to pilocarpine-induced epileptogenesis (Kong et al., 2012). Accordingly, it was hypothesized that compounds capable of increasing GLT-1 levels could have antiepileptic effects. Rothstein et al. (2005) first discovered that many β-lactam antibiotics, such as ceftriaxone, can increase GLT-1 levels through transcriptional activation. In a genetic model of epilepsy, early treatment with ceftriaxone showed antiepileptic effects (Zeng et al., 2010). Kong et al. (2014) reported that a small molecule, LDN/OSU-0212320, increased GLT-1 expression through translational activation. LDN/OSU-0212320 reduced the frequency of spontaneous seizures by 50% in a pilocarpine-induced TLE model. These findings further support the hypothesis that positive modulators of GLT-1 expression have the potential to treat epilepsy.

However, the question of why GLT-1 is lost has not yet been addressed. A previous study demonstrated that the loss is probably caused by disturbances at the posttranscriptional level because *GLT-1* mRNA is not decreased (Bristol and Rothstein, 1996). Studies on ALS cell models have found that mutant SOD1 causes down-regulation of GLT-1 by increasing the internalization and degradation of the surface transporter (Susarla and Robinson, 2008). This evidence suggests that excessive protein degradation may be the main cause of GLT-1 deficiency. If so, the antiexcitotoxicity effects achieved by promoting GLT-1 transcription or translation will be limited because excessive GLT-1 degradation will continue (Susarla and Robinson, 2008). Therefore, it is important to understand the molecular mechanisms underlying GLT-1 degradation.

Hsp90 is the most highly expressed cellular protein involved in the stabilization of other proteins and protein degradation under environmental stress (Whitesell and Lindquist, 2005). A recent study reported that Hsp90 expression was increased in neurons and glial cells of the dentate gyrus (DG) and CA1 in TLE (Kandratavicius et al., 2014). Although the

*L. Sha and X. Wang contributed equally to this paper.

Correspondence to Qi Xu: xuqi@pumc.edu.cn

Abbreviations used: 17AAG, 17-allylamino-17-demethoxygeldanamycin; AAV, adeno-associated virus; AED, antiepilepsy drug; CHX, cycloheximide; CKO, conditional KO; DG, dentate gyrus; ECF, extracellular fluid; EEG, electroencephalogram; FS, febrile seizure; GA, geldanamycin; HS, hippocampal sclerosis; IHC, immunohistochemistry; IR, immunoreactivity; KA, kainic acid; PLA, proximity ligation assay; PMV, plasma membrane vesicle; SE, status epilepticus; SFD, seizure-free day; SRS, spontaneous recurrent seizure; TLE, temporal lobe epilepsy; TSC, tuberous sclerosis complex.

The Rockefeller University Press $30.00
J. Exp. Med. 2017 Vol. 214 No. 2 547–563
https://doi.org/10.1084/jem.20160667

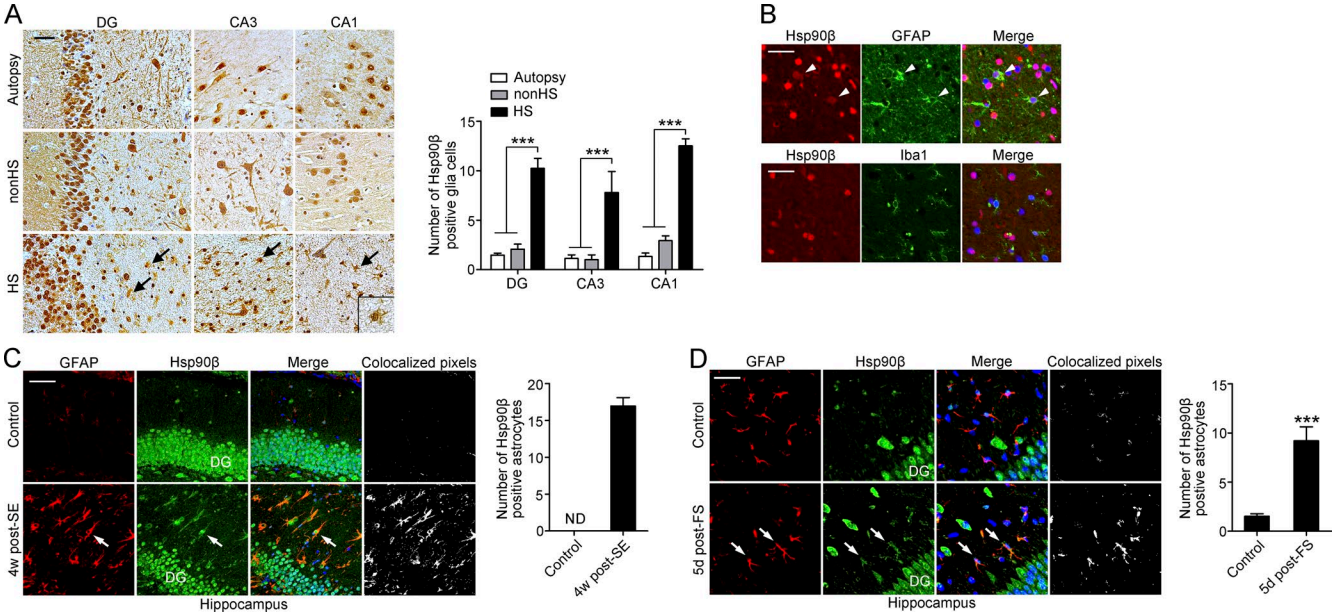

Figure 1. **Hsp90β is up-regulated in reactive astrocytes in the hippocampus of HS and mouse models of TLE and FS.** (A) Immunohistochemical staining for Hsp90β in the DG, CA1, and CA3 region of autopsy control, nonHS, and HS. Arrows indicate glia-likes cells in the sclerotic hippocampus (left; autopsy, $n = 5$; nonHS, $n = 5$; HS, $n = 7$). Bar, 50 µm. Quantification of Hsp90β$^+$ glia-like cells (right; ***, $P < 0.001$, Student's t test). (B) Representative images of the hippocampus from HS immunostained with Hsp90β (red), with an astrocyte-specific antibody GFAP (green), or with microglia-specific antibody Iba1 (green). Merged images revealed co-localization of Hsp90β with GFAP in astrocytes and a lack of co-localization of Hsp90β with Iba1 in microglia. Bar, 10 µm. (C) Immunofluorescence of Hsp90β and GFAP in the sclerotic hippocampus of mice at 4 wk after SE and in the saline injected control hippocampus (left). Quantification of Hsp90β$^+$ GFAP cells (right; $n = 4$ mice per group). Bar, 25 µm. (D) Immunofluorescence of Hsp90β and GFAP in the hippocampus of mice 5 d after experimental prolonged FS (left). Cell counting was performed under 40× magnification. Quantification of Hsp90β$^+$ GFAP cells (right; $n = 4$ mice per group; ***, $P < 0.001$, Student's t test). Bar, 15 µm. Data are representative of two independent experiments.

Hsp90 inhibitor exhibited neuroprotective effects in many animal models of neurological disorders (Luo et al., 2010), the molecular functions of Hsp90 in the nervous system, especially in astrocytes, are still poorly understood. In this study, we explored the role of Hsp90 in TLE and demonstrated that pharmacologic inhibition of Hsp90 to prevent GLT-1 degradation is a promising therapeutic strategy for TLE and related neurodegenerative disorders.

RESULTS

Hsp90β is up-regulated in astrocytes of human epileptogenic tissue

In mammalian cells, there are two major forms of cytosolic Hsp90, Hsp90α and Hsp90β. These proteins are highly homologous, but they exhibit divergent responses to environmental stimulation (Chen et al., 2005). We first examined the expression pattern of Hsp90 in autopsy control hippocampi, nonhippocampal sclerosis controls (nonHS), and hippocampal sclerosis (HS) in patients with drug-resistant TLE. In autopsy control hippocampi, the immunoreactivity (IR) of Hsp90α and Hsp90β was present throughout all subfields of the hippocampus. For Hsp90β, strong staining was present in the soma of neurons and along their neurites (Fig. 1 A). In addition to cytoplasmic staining, Hsp90β was also abundantly expressed in the nuclei of neurons. A similar expression pattern of Hsp90α and Hsp90β in neurons was observed in nonHS and HS hippocampi. However, compared with autopsy and nonHS controls, a substantially increased number of glia-like cells with Hsp90β IR was observed in the DG and CA1-CA3 subfields in HS (Fig. 1 A, arrows). This glial expression of Hsp90β in HS was co-labeled with GFAP in the cytoplasm but not Iba1 (Fig. 1 B), indicating that increased Hsp90β was predominantly in astrocytes. In contrast, immunohistochemical staining of Hsp90α was hardly detected in cells with glial morphology in all three groups of samples (Fig. S1 A), suggesting that Hsp90β, but not Hsp90α, is up-regulated in astrocytes in HS.

Expression of Hsp90β in mouse models of TLE and febrile seizures (FSs)

Having characterized a specific pattern of Hsp90β expression in hippocampal specimens of subjects with drug-resistant TLE, we looked for a similar pattern in the hippocampus of mouse models of epilepsy. We first used the established post-status epilepticus (SE) model of TLE, in which seizure activity develops within 1 wk after intrahippocampal application of 200 ng kainic acid (KA; Bouilleret et al., 1999). In the saline-injected control hippocampus, intensive Hsp90β IR was observed in the nuclei of granule cells in the DG, but no astrocytes were Hsp90β$^+$ (Fig. 1 C). At the chronic

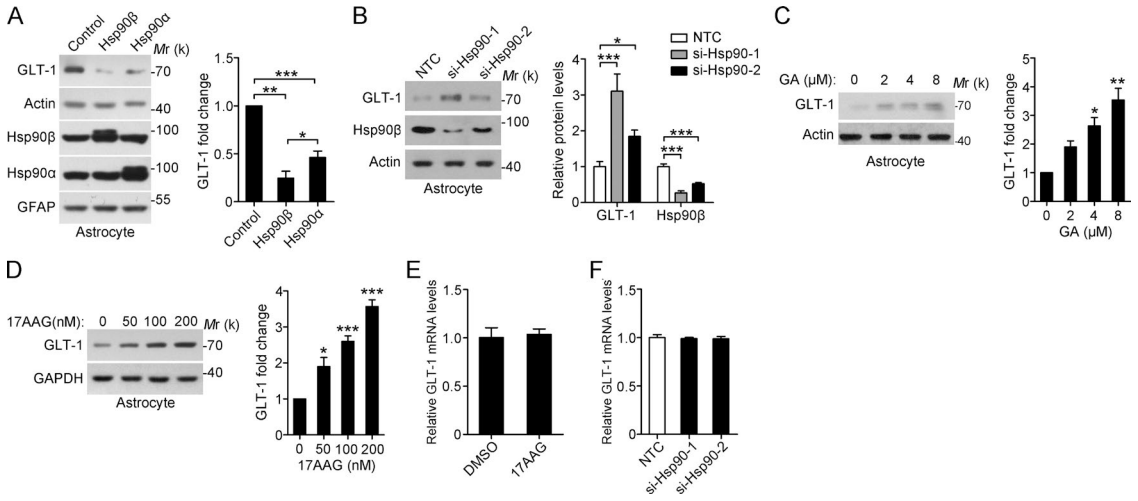

Figure 2. **Hsp90β negatively regulates GLT-1 protein levels.** (A) Western blot of astrocytes after lentivirus-mediated Hsp90α or Hsp90β overexpression for 72 h. Lentivirus expressing GFP was used as a control (left). Bar graph shows relative fold change of GLT-1 (right; normalized to actin; $n = 3$; *, $P < 0.05$; **, $P < 0.01$; ***, $P < 0.001$, Student's t test). (B) Western blot of astrocytes at 48 h after transfection with two independent siRNAs against Hsp90 (40 nM; left). Bar graph shows relative fold change of GLT-1 and Hsp90β (right; normalized to actin; $n = 3$; *, $P < 0.05$; ***, $P < 0.001$, Student's t test). (C and D) Western blot and statistical analysis of astrocytes with treatment of (C) GA or (D) 17AAG at different concentrations for 48 h ($n = 3$ for each group; *, $P < 0.05$; **, $P < 0.01$; ***, $P < 0.001$, one-way ANOVA, post hoc Dunnett's test). (E and F) Expression of *GLT-1* mRNA levels in astrocytes with treatment of 17AAG (100 nM, 24 h) and Hsp90 siRNA (40 nM, 48 h; Student's t test). NTC, nontarget control. Data are representative of at least two independent experiments.

stage post-KA–induced SE (examined at 4 and 16 wk), the sclerotic hippocampus ipsilateral to the KA injection displayed substantially increased Hsp90β IR in the cytoplasm of GFAP-labeled astrocytes, which was accompanied by reactive astrogliosis (Fig. 1 C and Fig. S1 B). Hsp90β$^+$ astrocytes were also observed to be widely distributed in the early stage after KA injection (examined on days 1, 5, and 10; Fig. S1 C), suggesting a long-lasting activation of Hsp90β in astrocytes from the transition of quiescent astrocytes to reactive astrocytes.

A striking correlation was found in TLE patients with a frequent history of childhood FS (Harvey et al., 1995). Thus, we examined whether Hsp90β can be induced in astrocytes by experimentally prolonging FS (Dubé et al., 2006). As expected, the number of Hsp90β$^+$ astrocytes in the hippocampus was significantly increased after FS compared with controls (Fig. 1 D). Finally, using an in vitro model of astrogliosis induced by TGFβ (Yu et al., 2012), we observed that Hsp90β was up-regulated after astrocytes transitioned from a quiescent to a reactive state, as indicated by increased GFAP expression (Fig. S1 D). Collectively, our result indicates a specific activation of Hsp90β in reactive astrocytes after an excitotoxic lesion.

Hsp90β negatively regulates GLT-1 protein levels

Given that Hsp90β levels are closely related to the reactive state of astrocytes, we sought to investigate whether up-regulation of Hsp90β underlies the impaired glutamate-buffering capability. Using lentivirus-mediated gene transfer into primary cultured astrocytes, we found that Hsp90β overexpression resulted in a notable decrease in GLT-1 protein levels (Fig. 2 A). Although the expression of Hsp90α in astrocytes is not changed in the sclerotic hippocampus of TLE patients, overexpression of Hsp90α also reduced GLT-1 levels, but to a lesser extent than overexpression of Hsp90β (Fig. 2 A). Neither Hsp90α nor Hsp90β affected GFAP levels (Fig. 2 A). In contrast, knockdown of Hsp90 significantly increased expression of GLT-1 (Fig. 2 B). We examined the effects of Hsp90 inhibitor geldanamycin (GA), and its less toxic analogue 17-allylamino-17-demethoxygeldanamycin (17AAG) on GLT-1 protein levels (Miyata, 2005). Similarly, inhibition of Hsp90 by GA or 17AAG increased GLT-1 levels in a concentration-dependent manner (Fig. 2, C and D). However, treatment with 17AAG or Hsp90 siRNA did not affect the expression of *GLT-1* mRNA (Fig. 2, E and F), suggesting that Hsp90 regulates GLT-1 expression at the post-transcriptional level. Consistent with this finding, 17AAG up-regulated exogenous GLT-1 in 293t cells transfected with GLT-1-myc (Fig. S2 A).

Moreover, inhibition of Hsp90 has no effect on the levels of GLAST, xCT, and GFAP (Fig. S2 B). Hsp70 can exert opposing roles on Hsp90 substrates, and Hsp90 inhibition is always accompanied by up-regulated Hsp70 expression (Fig. S2 B). However, we did not observe any change in GLT-1 levels when astrocytes were treated with Hsp70 inhibitor (Fig. S2 C). Collectively, our data demonstrate that Hsp90β negatively regulates the protein expression of GLT-1 in astrocytes.

17AAG increases the stability of GLT-1 by disrupting Hsp90β–GLT-1–20S proteasome association

Next, we sought to identify the mechanism of Hsp90β-induced GLT-1 reduction. As previously reported, GLT-1 is

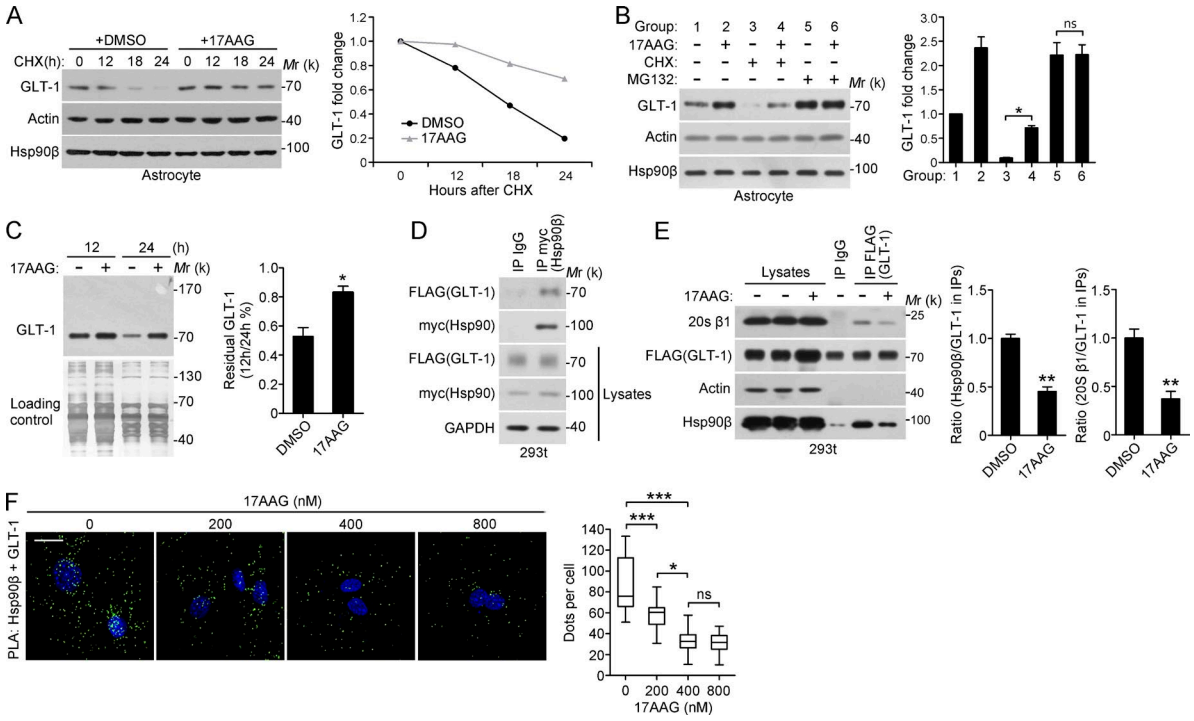

Figure 3. **GLT-1 binds to Hsp90β, and 17AAG prevents GLT-1–Hsp90β–20S proteasome assembly.** (A) Representative Western blot of astrocytes treated with DMSO or 17AAG (100 nM) in the presence of CHX (50 µg/ml) before harvesting (left). (right) Quantification of band intensities (normalized to actin and the t = 0 time point; $n = 3$). (B) Representative Western blot of astrocytes treated with 17AAG (100 nM), CHX (50 µg/ml), MG132 (10 µM), or both for 24 h, as indicated (left). Statistical analysis of GLT-1 expression (right; *, $P < 0.05$, Student's *t* test). (C) Representative Western blot of the pulse–chase analysis. Astrocytes were preincubated with sulfo-NHS-SS-biotin for 30 min to label surface proteins and were then treated with DMSO or 17AAG (400 nM; $n = 3$; *, $P < 0.05$, Student's *t* test). Equal protein loading was confirmed by silver staining. (D) Representative Western blot analysis for GLT-1-FLAG after the immunoprecipitation of Hsp90β-myc. 293t cells were cotransfected with Hsp90β-myc and GLT-1-FLAG for 48 h and lysed for immunoprecipitation with an anti-myc antibody. (E) Representative Western blot analysis for Hsp90β-myc after immunoprecipitation of GLT-1-FLAG ($n = 3$). 293t cells were cotransfected with Hsp90β-myc and GLT-1-FLAG. 6 h after transfection, the cells were treated with or without 17AAG for 42 h (right; normalized to actin; **, $P < 0.01$, Student's *t* test). (F) PLA assay for GLT-1-Hsp90β association in astrocytes treated with 17AAG at different concentrations for 48 h. The nuclei were stained with DAPI (blue). The data are expressed as the median, the 25th–75th percentile (box), or the min-max percentile (whiskers; $n = 3$; *, $P < 0.05$; ***, $P < 0.001$, one-way ANOVA, Tukey's post hoc test). Bar, 10 µm. Data are representative of at least two independent experiments.

a relatively stable protein. Cycloheximide (CHX) treatment decreased GLT-1 levels, whereas the decrease in GLT-1 levels under CHX treatment was partially rescued by the addition of 17AAG (Fig. 3 A). GLT-1 can be ubiquitinated and degraded by the proteasome (García-Tardón et al., 2012), whereas treatment of astrocytes with the proteasome inhibitor MG132 elevated GLT-1 levels (Fig. 3 B, line 1 vs. 5). Furthermore, incubation with MG132, 17AAG, or their combination led to a similar accumulation of GLT-1 protein (Fig. 3 B, lines 2, 5, and 6), indicating that the increase in GLT-1 levels are a consequence of inhibited proteasome-dependent GLT-1 degradation. Pulse-chase experiments also demonstrated that Hsp90 inhibition can prevent GLT-1 degradation (Fig. 3 C). However, the ubiquitination of GLT-1 was not influenced by either Hsp90β overexpression or 17AAG (Fig. S3 A), suggesting that Hsp90β affects GLT-1 levels independently of its ubiquitination status. To further confirm this assumption, we generated GLT-1 K-to-R mutants in which all 31 lysine residues were replaced with arginine. In the transfected 293t cells, although K-to-R mutants cannot be ubiquitinated like wild-type GLT-1, 17AAG treatment still up-regulated GLT-1 protein levels (Fig. S3 B). Together, these experiments strongly suggest the involvement of Hsp90β in regulating GLT-1 proteasome degradation.

Because substrate binding is the most common mechanism through which Hsp90 interacts with its target proteins, we examined whether GLT-1 interacts with Hsp90β. In 293t cells transfected with Hsp90β-myc and GLT-1-FLAG, we found that Hsp90β coimmunoprecipitated with GLT-1 (Fig. 3 D). In addition, GLT-1 coimmunoprecipitated with Hsp90β from the ipsilateral hippocampus of KA-injected mice (Fig. S3 C). Furthermore, 17AAG treatment disrupted the interaction between Hsp90β and GLT-1 (Fig. S3 D). To analyze the association of GLT-1 with Hsp90β through a complementary approach, we used proximity ligation assays (PLA) to detect endogenous GLT-1–Hsp90β complexes in primary cultured astrocytes. The specificity of the PLA signal was confirmed by knocking down Hsp90 or GLT-1 in astro-

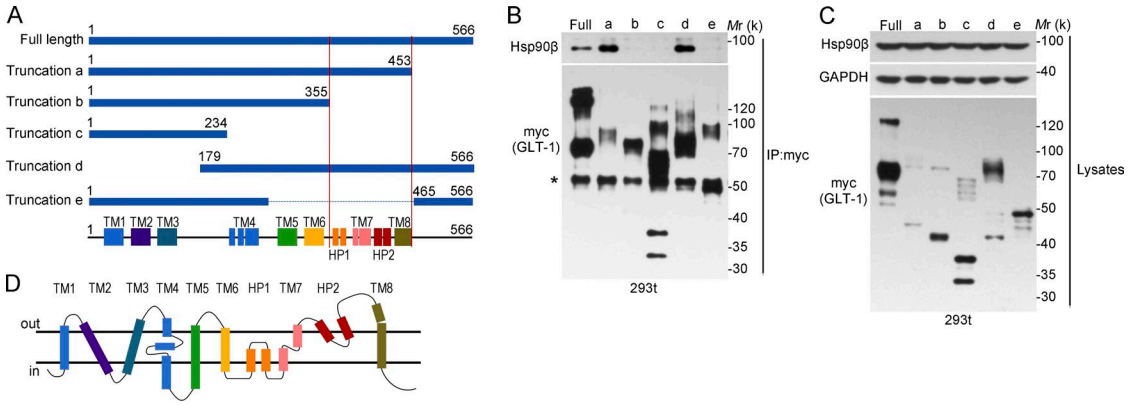

Figure 4. **The interaction between GLT-1 and Hsp90β.** (A) Illustration of GLT-1 truncations. The region between two red lines is indispensable for GLT-1 and Hsp90β interaction (B and C) Representative Western blot analysis for Hsp90β-FLAG after immunoprecipitation of full-length GLT-1-myc and truncations ($n = 3$). 293t cells were transfected with full-length GLT-1 or truncated GLT-1 (a–e). Asterisk indicates IgG heavy chain. (D) Structural features of the mammalian GLT-1 in lipid bilayer. All data are representative of at least three independent experiments. TM, transmembrane; HP1, 2, hairpin (HP) loops 1, 2. All experimental data were verified in two independent experiments.

cytes (Fig. S3 F). As expected, the number of dots that represented the in situ GLT-1–Hsp90β complexes was decreased by 32.2 and 61.2% after 17AAG treatment at 200 and 400 nM, respectively (Fig. 3 F). Treatment with 800 nM 17AAG did not result in a further reduction in the number of GLT-1–Hsp90β complexes (62.7%; Fig. 3 F).

Previous evidence has demonstrated that Hsp90 directly binds the 20S proteasome (Eleuteri et al., 2002). Indeed, we found that a subunit of the 20S proteasome is a component of the GLT-1–Hsp90β complex (Fig. 3 E). Like the association between GLT-1 and Hsp90β, the interaction between GLT-1 and the 20S proteasome was also disrupted by 17AAG treatment (Fig. 3 E). These data indicated that Hsp90β may promote the association between GLT-1 and the 20S proteasome, leading to GLT-1 degradation. Consistent with this model, the interaction between endogenous GLT-1 and the 20S proteasome subunit in astrocytes can be detected after inhibition of the 20S proteasome activity by MG132 (Fig. S3 E).

Further characterization of this protein interaction revealed that deletion of the GLT-1 C-terminal 356–453 aa abolished the binding of GLT-1 to Hsp90β (Fig. 4, A and B). Although the protein levels of GLT-1 truncation fragments containing 356–453 aa were much lower, their interaction with Hsp90β were stronger than that for the full-length GLT-1 (truncation-a, d; Fig. 4, B and C), indicating that this region is responsible for Hsp90β-dependent GLT-1 degradation. Collectively, our data suggest that Hsp90β recruits GLT-1 to the 20S proteasome, thereby promoting GLT-1 degradation.

17AAG enhances glutamate uptake in astrocyte cultures

Next, we tested whether the inhibition of Hsp90 could enhance the ability of astrocytes to remove extracellular glutamate in vitro. Functional GLT-1 is expressed as a multimer comprising three noncovalently associated GLT-1 monomers (Vandenberg and Ryan, 2013). Treatment of astrocytes with 17AAG caused significant accumulation of GLT-1 in both membrane and cytosolic extracts (Fig. 5 A). To explore whether Hsp90 inhibition affected the absorption of glutamate by astrocytes, glutamate uptake with [^{3}H]-glutamate was performed in cultured astrocytes, and DHK, a GLT-1 inhibitor, was used to distinguish GLT-1–mediated glutamate uptake from that of other glutamate transporters. The results showed that DHK-sensitive, Na^+-dependent ^{3}H-glutamate uptake activity was significantly increased in 17AAG and Hsp90-siRNA–pretreated astrocytes (Fig. 5, B and C). In contrast, overexpression of Hsp90β impaired glutamate uptake activity (Fig. 5 D). It is worth noting that the DHK-insensitive, Na^+-dependent ^{3}H-glutamate uptake activity was not influenced in the aforementioned three groups (0.64 ± 0.05 DMSO vs. 0.57 ± 0.05 17AAG; 0.55 ± 0.06 NTC vs. 0.57 ± 0.03 si-Hsp90; 0.46 ± 0.04 Control vs. 0.46 ± 0.05 Hsp90β pmol/mg protein/10 min). We also examined changes in extracellular glutamate concentration. Likewise, 17AAG treatment resulted in a more rapid decline in the extracellular concentration of unlabeled glutamate (short-term assay in Fig. 5 E and long-term assay in Fig. 5 F). In conclusion, our in vitro experiment demonstrated that 17AAG can prevent GLT-1 degradation and enhance the ability of astrocytes to remove extracellular glutamate.

17AAG exhibits an anticonvulsant effect in the acute seizure model

Given the potential role of up-regulated Hsp90β in accelerating GLT-1 degradation in TLE, we next examined whether 17AAG has anticonvulsant activity. To test this possibility, we first assessed the effect of 17AAG on GLT-1 protein levels in vivo. Male C57BL6 mice received i.p. injection of 17AAG three times weekly for 1 wk, and their hippocampal extracts were analyzed by Western blot. The effect of 17AAG on GLT-1 levels was dose dependent, with the GLT-1 protein

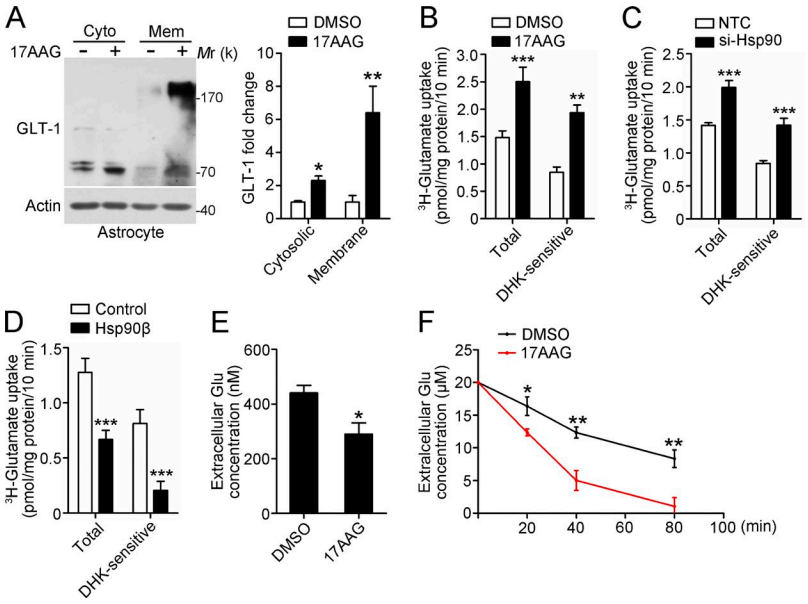

Figure 5. **17AAG enhances the glutamate clearance capacity of astrocytes in vitro.** (A) Representative Western blot analysis for membrane and cytosolic GLT-1 (left). Astrocytes were treated with 17AAG (100 nM, 48 h). The bar graph shows the relative fold change of GLT-1 (right; $n = 3$; *, $P < 0.05$; **, $P < 0.01$, Student's t test). (B–D) [^{3}H]-glutamate uptake analysis. Astrocytes were pretreated with 17AAG (B; 100 nM, 48 h; $n = 4$), Hsp90-siRNA (C; 40 nM, 48 h; $n = 5$), or Hsp90β lentivirus (D; 72 h; $n = 5$), and DHK (100 μM), a GLT-1 inhibitor, was added 1 h before the assays to distinguish DHK-sensitive glutamate uptake (**, $P < 0.01$; ***, $P < 0.001$, Student's t test). (E and F) Extracellular glutamate assay. 36 h after DMSO or 17AAG (100 nM) treatment, the astrocytes were depleted of glutamate for 12 h in Opti-MEM, and then incubated in an uptake buffer containing 500 nM or 20 μM unlabeled glutamate for (E) short-term or (F) long-term assays, respectively. Extracellular glutamate concentrations were determined in samples from the uptake buffer collected at the indicated time points ($n = 4$ for each group; *, $P < 0.05$, Student's t test in E; *, $P < 0.05$; **, $P < 0.01$, one-way ANOVA with post-hoc Dunnett's tests in F). All experimental data were verified in at least two independent experiments.

levels reaching a maximal level at 25 mg/kg (Fig. 6 A). Next, we examined the time course of the effects of 17AAG on GLT-1. The level of GLT-1 peaked at 12 h after injection and began to decrease thereafter; however, the level of GLT-1 was still 1.4-fold higher than the basal level at 48 h (Fig. 6 B). This finding is consistent with previous studies in which the effect of 17AAG on Hsp90-targeted proteins lasted up to 48 h (Egorin et al., 2001; Ramanathan et al., 2005).

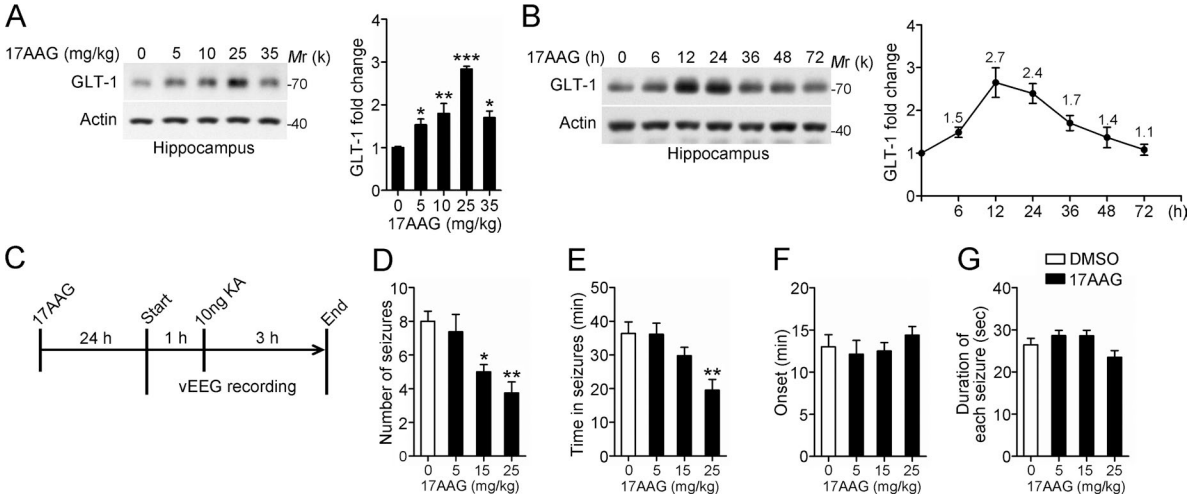

Figure 6. **The anticonvulsant effect of 17AAG in an acute seizure model.** (A) Representative Western blot of GLT-1 in the hippocampus of mice 24 h after receiving i.p. injection of 17AAG three times weekly for 1 wk at the indicated dose. Bar graph shows relative fold change of GLT-1 ($n = 4$ mice per group; *, $P < 0.05$; **, $P < 0.01$; ***, $P < 0.001$, one-way ANOVA, post hoc Dunnett's test). Data are representative of two independent experiments. (B) Western blot of GLT-1 in the hippocampus of 17AAG-injected mice at the indicated time point after 17AAG injection (25 mg/kg). Bar graph shows relative fold change of GLT-1 ($n = 3$ for each time point). Data are representative of two independent experiments. (C) Experimental protocol for drug testing in an acute seizure model. Wild-type mice implanted with a hippocampal electrode and cannula were injected once with 17AAG 24 h before testing. The first EEG recording period (1 h) was used to assess the baseline of EEG activity. The vEEG was then recorded continuously after intrahippocampal KA injection (10 ng KA in 0.5 μl of PBS) for 3 h. All mice were recovered from KA-induced acute seizures within 3 h. (D–G) The EEG data were analyzed, and the total number of seizures, the duration from the first to the last seizure event (Time in seizures), the onset time after KA injection, and mean duration of each seizure are presented ($n = 8$ mice per group; *, $P < 0.05$; **, $P < 0.01$, one-way ANOVA, post hoc Dunnett's test). Data are combined from four independent experiments.

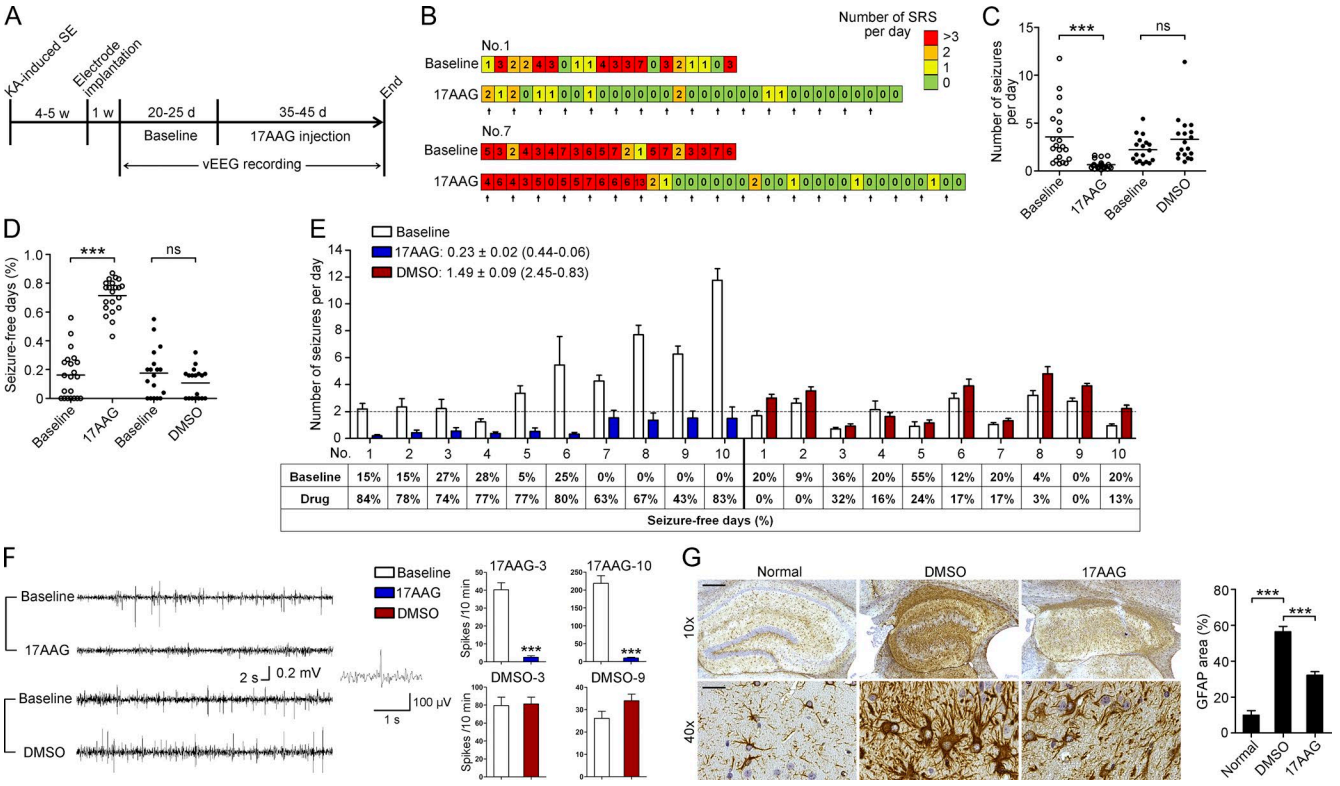

Figure 7. **The anticonvulsant effect of 17AAG in a TLE mouse model.** (A) Experimental design. (B) Example of daily recording of SRSs in the 17AAG group. (C and D) Statistical analysis of the number of seizures per day and seizure-free days. Cumulative data from four individual experiments with 18 mice in the DMSO group and 21 mice in the 17AAG group pooled per experiment (***, $P < 0.001$, Mann–Whitney test or Student's *t* test). (E) Number of seizures per day and percentage of seizure-free days in the first 10 mice of the 17AAG and DMSO groups, respectively. The average fold change in seizure frequency in individual mice before and after administration was 0.23 ± 0.02 (0.44–0.06) in the 17AAG group ($n = 21$) and 1.49 ± 0.09 (2.45–0.83) in the DMSO group ($n = 18$). (F) Representative 1-min EEG tracings recorded from mice during the preinjection baseline and during drug injection in the 17AAG and DMSO groups, respectively. Statistical analysis of interictal spikes from two mice in each group are presented (***, $P < 0.001$, Student's *t* test). (G) Representative images of GFAP staining in the sclerotic hippocampus and statistical analysis (Normal, $n = 6$; DMSO, $n = 8$; 17AAG, $n = 8$, ***, $P < 0.001$, one-way ANOVA, post hoc Tukey's test). Data are from two individual experiments (G). Bars: (top) 100 µm; (bottom) 30 µm. Data are representative of two (G) independent experiments.

Next, we applied pharmacological interference to an acute model of epilepsy (Maroso et al., 2010). At 24 h after mice received 17AAG injection (Fig. 6 C), acute seizures were induced by intrahippocampal application of 10 ng KA. This dose induced epileptic seizures in 100% of mice without any mortality. This result demonstrates a dose-dependent anticonvulsant effect of 17AAG in wild-type mice. At 15 and 25 mg/kg, the total number of acute seizures was significantly reduced compared with the vehicle group (DMSO-injected WT littermates; Fig. 6 D). The time in seizures was also significantly decreased at 25 mg/kg (Fig. 6 E). However, preinjection with 17AAG did not affect the time of onset of the first seizure or duration of each seizure (Fig. 6, F and G).

17AAG reduces chronic seizures and ameliorated astrogliosis in mouse models of TLE

Next, using the post-SE model of TLE, we investigated whether 17AAG exerted antiepileptic effects in mice that had already developed spontaneous seizures. This model is most similar to human refractory TLE and is used for preclinical drug screening of antiepilepsy drugs (AEDs; Rattka et al., 2013).

Fig. 7 A illustrates the experimental procedures. Because mice with a low seizure frequency may occasionally become seizure-free for at least several days, only animals that had at least four motor seizures per week were chosen for subsequent analyses. During drug injection and the following vEEG monitoring, three mice in the 17AAG group and two mice in the DMSO group died from lethal seizures. At the end of the experiment, vEEG data were analyzed for 21 and 18 mice in the 17AAG and DMSO groups, respectively.

17AAG was administered at 25 mg/kg once every other day, and WT littermates were injected with DMSO. Most of the mice exhibited an apparent reduction in seizure frequency (number of seizures per day) after receiving four to eight 17AAG injections (Fig. 7 B). The administration of 17AAG dramatically suppressed epileptic seizures to 0.81 ±

0.76 per day, a mean decrease of 77% compared with baseline (Fig. 7 C). In contrast, although this result was not statistically significant, the seizure frequency in the DMSO group was increased 1.5-fold before and after DMSO injection (Fig. 7 C). The quantification of the number of seizure-free days (SFDs) is another important evaluation of AEDs. The percentage of SFDs during baseline in the 17AAG group was 14.9% and increased to 74.1% during 17AAG treatment (Fig. 7 D). In comparison, the SFDs in the DMSO group decreased from 22.0% to 13.6% (Fig. 7 D). The changes in seizure frequency of individual animals are shown in Fig. 7 E and Fig. S4 A. The inhibitory effect of 17AAG on the spontaneous seizure activity among the individual animals varied from 52 to 94% (mean, 73.4 ± 2.7%), but this effect was not correlated with the baseline seizure activity (Pearson's r = 0.13; P = 0.1036). Although the duration of each EEG seizure remained unchanged (Fig. S5 A), 17AAG treatment substantially decreased the interictal epileptiform discharges (Fig. 7 F and Fig. S4 B), indicating that the glutamate levels in hippocampal extracellular fluid (ECF) were reduced. Indeed, in vivo hippocampal microdialysis revealed a dramatic reduction in the ECF glutamate concentration in the 17AAG group when compared with the DMSO group (1.26 ± 0.09 nM DMSO vs. 0.82 ± 0.05 nM 17AAG; Fig. S5, B–D). Consistent with the aforementioned results, the glutamate uptake function was improved in the hippocampal plasma membrane vesicles (PMVs) of the 17AAG-treated mice (Fig. S5 E).

In addition, three mice received 17AAG injection for 120 d. The inhibitory effect of 17AAG on spontaneous seizure activity was 72, 93, and 91%, a mean decrease of 85% compared with baseline. There was no evidence of drug resistance in the treated mice. As previously reported (Waza et al., 2005), we found that 17AAG did not cause neuronal loss or glial activation in the mice after long-term low-dose treatment (Fig. S4 C). Collectively, our data suggest that 17AAG can be used as a long-term therapeutic intervention in TLE.

We further compared ceftriaxone (200 mg/kg), which increases GLT-1 expression through transcriptional activation (Macaluso et al., 2013; Kong et al., 2014), to 17AAG (25 mg/kg), which blocks GLT-1 degradation. As shown in Fig. S5 F, 17AAG corresponded to a greater GLT-1 induction than ceftriaxone. Moreover, ceftriaxone-treated mice exhibited a lower seizure frequency than baseline (Fig. S5 G), although this difference was not statistically significant. Overall, 17AAG treatment that inhibits GLT-1 degradation is effective in suppressing spontaneous recurrent seizures (SRSs).

To assess whether the reduced SRS was accompanied by reversed histological abnormalities in the sclerotic hippocampus, mice were euthanized for pathological diagnosis once vEEG monitoring concluded. Timm's staining was used to evaluate the degree of aberrant mossy fiber sprouting, but there was no difference between the DMSO and 17AAG groups (Fig. S5 H). Moreover, treatment with 17AAG did not affect ectopic granule cells (Fig. S5 I). Finally, we assessed astrogliosis by GFAP staining. Quantification of GFAP immunostaining revealed that although reactive astrogliosis was prominent in sclerotic hippocampi compared with normal hippocampi, there was a dramatic decrease in the area occupied by astrocytes in 17AAG-treated mice (Fig. 7 G). These findings suggest that long-term 17AAG treatment to inhibit SRS can subsequently ameliorate astrogliosis in mouse models of TLE, further supporting reactive astrogliosis as a therapeutic target for HS.

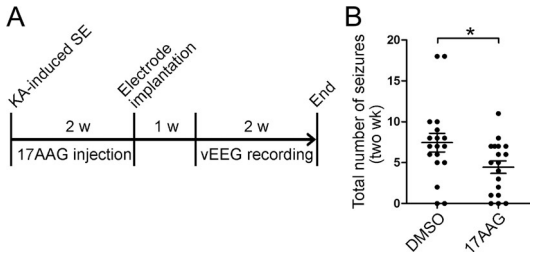

Figure 8. **The effect of 17AAG on temporal lobe epileptogenesis.** (A) Experimental design. 24 h after KA-induced SE, mice were injected with 17AAG once every other day for 2 wk; littermate WT mice were injected with DMSO. Thereafter, mice were implanted with electrodes and followed for 2 wk using vEEG recording without drug intervention. (B) Statistical analysis of the total number of seizures in the two recording weeks (n = 18 mice per group; *, P < 0.05, Student's t test). Data are combined from two independent experiments.

Glutamate-transporter impairment in astrocytes directly contributes to the epileptogenic process. Therefore, we injected 17AAG into mice for 2 wk after the onset of SE and then examined their SRS over the following 2 wk without intervention to assess whether 17AAG affects temporal lobe epileptogenesis (Fig. 8 A). The incidence of epilepsy was not affected (16/18 DMSO vs. 15/18 17AAG); however, the mean number of seizures over the two recording weeks was reduced in the 17AAG-treated group (7.4 ± 1.1 DMSO vs. 4.4 ± 0.8 17AAG; Fig. 8 B). These results suggest that excessive glutamate in the epileptic brain is necessary but not sufficient for the establishment of aberrant neural circuits. Collectively, our data strongly suggest that 17AAG exhibits an anticonvulsant effect in mice with chronic spontaneous epilepsy and therefore has a disease-modifying effect.

AAV5-mediated Hsp90β transfer to astrocytes exacerbated seizures and can be rescued by 17AAG

Given the anticonvulsant effect of Hsp90 inhibitor, we further tested whether overexpression of Hsp90β in astrocytes could exacerbate seizures in mice with chronic epilepsy. Recombinant adeno-associated virus 5 (AAV5) expressing Hsp90β was constructed and infused into the hippocampus ipsilateral to KA injection to deliver Hsp90β to astrocytes. The experimental procedures are illustrated in Fig. 9 A and presented in detail in the Materials and methods. Compared with the seizure frequency of each animal at baseline, injection of AAV5-Hsp90β led to a 2.84 ± 0.40-fold increase in seizure frequency (range, 1.8–4.4), which was significantly

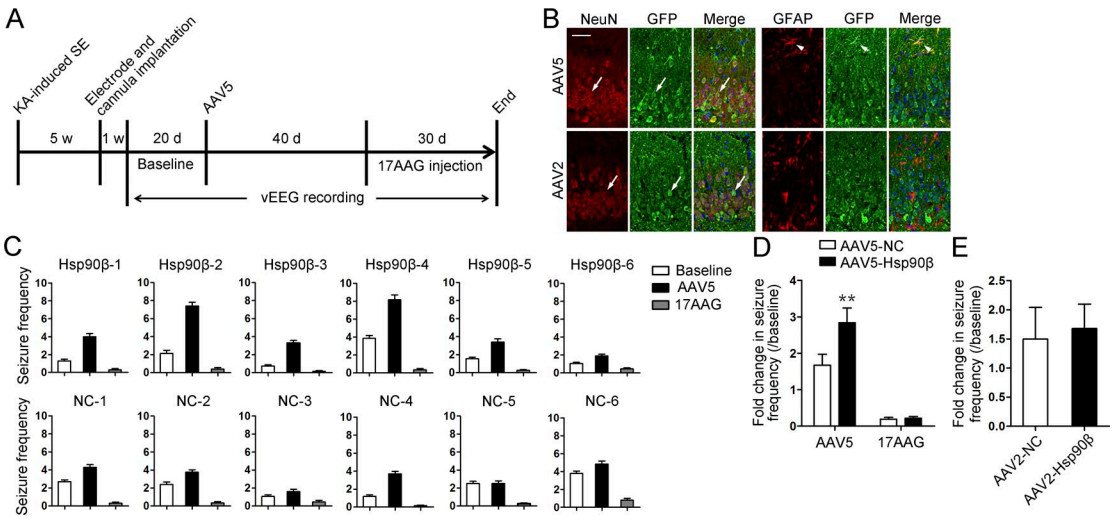

Figure 9. **AAV5-mediated Hsp90β expression in astrocytes demonstrated a proconvulsant effect in the TLE model.** (A) Experimental design. (B) AAV2-GFP or AAV5-GFP was injected into the sclerotic hippocampus to show cell type–specific expression. Representative images of GFP and GFAP or of GFP and NeuN staining in the AAV5-GFP– and AAV2-GFP–injected sclerotic hippocampus, respectively. Merged images revealed co-localization of GFP with GFAP in the AAV5-injected hippocampus (arrowheads) and the co-localization of GFP with NeuN in both the AAV2- and AAV5-injected hippocampus (arrows). Bar, 50 µm. (C) Seizure frequency was measured from the EEG data recorded during baseline (open columns) during the last 20 d after AAV5 injection (filled columns) and during the last 20 d after 17AAG injection (gray columns). (D) The fold change in seizure frequency after AAV5 or 17AAG injection was determined ($n = 6$ for each group; **, $P < 0.01$, Student's t test). Data are combined from two independent experiments. (E) The fold change in seizure frequency after AAV2 injection (AAV2-NC, $n = 4$; AAV2-Hsp90β, $n = 6$ mice). Data are representative of two independent experiments. Seizure frequency, mean number of seizures per day; NC; negative control; SE, status epileptic.

higher than the value in the AAV5-NC group (1.67 ± 0.30; range, 1.0–3.1). However, the seizure frequencies in both groups were suppressed to a similar degree by 17AAG treatment (seizure frequency: 0.38 ± 0.09 AAV5-NC vs. 0.32 ± 0.04 AAV5-Hsp90β. Fig. 9, C and D). As previously reported (Weinberg et al., 2011), AAV5 can also be used to deliver genes to hippocampal neurons (Fig. 9 B), but we did not observe marked changes in the seizure frequency after intrahippocampal injection of AAV2-Hsp90β compared with the AAV2-NC group (Fig. 9 E). Because AAV2 delivers genes specifically to neurons (Fig. 9 B), it can be concluded that the expression of Hsp90β in hippocampal neurons is not related to the generation of spontaneous seizures. In summary, we demonstrated that the up-regulation of Hsp90β in astrocytes induces proconvulsant effect in TLE.

17AAG provides neuroprotective effects in a mouse model of tuberous sclerosis

Seizures are the initial manifestation of tuberous sclerosis complex (TSC) and often refractory to AEDs. We next tested the effects of 17AAG in *Tsc1*$^{flox/flox}$;GFAP-Cre conditional knockout mice (*Tsc1*^{GFAP}CKO), a well-established mouse model of TSC (Uhlmann et al., 2002). The treatment of 17AAG or DMSO was initiated at postnatal day 14, which precedes the onset of epilepsy in *Tsc1*^{GFAP}CKO mice. Compared with DMSO-treated *Tsc1*^{GFAP}CKO littermate controls, 17AAG treated mice had significantly prolonged survival rate (Fig. 10 A). Spontaneous seizures start to develop in *Tsc1*^{GFAP}CKO mice at 4–5 wk of age and become progressively more frequent over the ensuing months (Zeng et al., 2010). We monitored the motor seizures by videotaping *Tsc1*^{GFAP}CKO mice for 2 wk, starting at 6 wk of age. By comparison, 17AAG-treated *Tsc1*^{GFAP}CKO mice exhibited significantly decreased seizure frequency compared with DMSO-treated *Tsc1*^{GFAP}CKO mice (Fig. 10 B). These findings suggest that 17AAG can also offer neuroprotective and anti-epileptic effects in genetic epilepsy.

DISCUSSION

In this study, we demonstrated that Hsp90β interacts with GLT-1 and recruits it to 20S proteasome for degradation. The Hsp90 inhibitor 17AAG can prevent proteasome-dependent GLT-1 degradation by disrupting the Hsp90β–GLT-1 association, and it exhibits a considerable anticonvulsant effect in both acquired and genetic forms of epilepsy (Fig. 10 C).

In neurodegenerative disorders, including ALS, AD, and TLE, insufficient GLT-1 is considered to be the main cause of excitotoxicity (Lin et al., 2012). Accordingly, restoring GLT-1 protein levels and functions may provide therapeutic benefits for excitotoxicity in these chronic diseases. Ceftriaxone is the first drug to induce GLT-1 expression via transcriptional activation. However, although GLT-1 protein levels were substantially increased in vitro, ceftriaxone treatment showed no therapeutic effect in ALS or chronic epilepsy (Zeng et al., 2010; Cudkowicz et al., 2014). One possible explanation for this ineffectiveness is that excessive GLT-1 degradation in

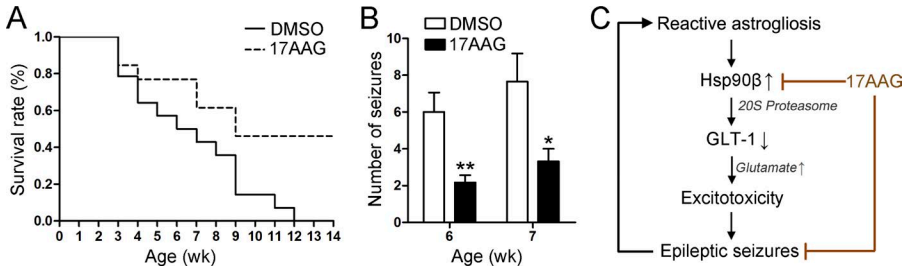

Figure 10. **17AAG treatment improves survival and decreases seizures in *Tsc1*^{GFAP}CKO mice.** (A) The survival rate revealed that 50% of the DMSO-treated *Tsc1*^{GFAP}CKO mice died by 6 wk of age, and all died by ∼12 wk of age. In contrast, 17AAG treatment significantly increased the survival rate of the *Tsc1*^{GFAP}CKO mice (P = 0.0146, Kaplan-Meier log-rank test). Cumulative data from two individual experiments with 13 DMSO-treated mice and 14 17AAG-treated mice pooled per experiment. (B) Statistical analysis of the total number of seizures in 6–7 wk of age (n = 6 mice per group, *, P < 0.05; **, P < 0.01, Student's t test). Data are representative of two independent experiments. (C) Schematic representation of Hsp90β-mediated GLT-1 degradation and the anticonvulsant effect of 17AAG.

disease conditions neutralizes the efforts to increase GLT-1 expression. We assumed that the inhibition of GLT-1 degradation might be more effective for the treatment of excitotoxicity than for the promotion of GLT-1 expression. Our results support this idea. First, in the normal brain, the effects of 17AAG on GLT-1 expression are comparable to those of ceftriaxone and LDN/OSU-0212320, which increase the expression of GLT-1 by two- to three-fold (Fig. 6 A; Macaluso et al., 2013; Kong et al., 2014). However, in the epileptic hippocampus, 17AAG maintained GLT-1 protein levels more effectively than ceftriaxone. Second, 17AAG exhibited a remarkable seizure-suppressive effect in the TLE model and was more effective than either ceftriaxone or LDN/OSU-0212320 (Kong et al., 2014). Therefore, inhibition of excessive GLT-1 degradation may be an alternative treatment for TLE, and it may represent a more feasible way to restore GLT-1 levels in neurological disorders.

To date, little is known of the roles of Hsp90 molecules in astrocytes, whereas the neuroprotective effects of Hsp90 inhibitors in neurological diseases have been widely studied (Auluck et al., 2005; Waza et al., 2005; Fujikake et al., 2008). The beneficial effects of Hsp90 inhibitor in neurodegenerative diseases have been attributed to the inhibition of Hsp90 activity and increased Hsp70 levels in affected neurons. A change in the Hsp90/Hsp70 balance can redirect neuronal aggregate formation, reduce aberrant neuronal protein activity, and protect against excitotoxicity (Luo et al., 2010). In this study, we observed that Hsp90 inhibition prevents GLT-1 degradation in astrocytes through which 17AAG exerts antiepileptic and antiexcitotoxic effects. In fact, reactive astrogliosis is hallmark of many neurological disorders. In epilepsy, astrogliosis is thought to contribute directly to the generation of spontaneous seizures via impaired astrocytic glutamate uptake, whereas immunocytokines induced by epileptic seizures can in turn further promote the reactivity of astrocytes (Robel et al., 2015). Our results suggest a stress-inducible expression model of Hsp90β in astrocytes. Hsp90β is induced after the transition of quiescent astrocytes to the reactive phenotype, which subsequently leads to insufficient glutamate uptake by depleting GLT-1 (Fig. 10 C). It can be speculated that the neuroprotective mechanisms of Hsp90 inhibitors were previously underestimated, and it is worth reexamining the long-term therapeutic effects of 17AAG or its analogue in disease models in which excitotoxicity has been shown to contribute to neurodegeneration.

The Hsp90 inhibitor 17AAG is a less toxic and more stable analogue of GA. 17AAG is presently under extensive clinical research for use in antitumor therapy because it binds to Hsp90 and destabilizes target oncoproteins in tumor cells (Dimopoulos et al., 2011). The toxicity of 17AAG in reported trials was dose and schedule dependent, with hepatotoxicity being more prominent with daily administration. Other toxicities included primarily diarrhea and fatigue (Jhaveri et al., 2012). In the brain, Hsp90 is widely expressed in neurons and functionally interacts with a broad array of client proteins, such as Hsp70, androgen receptor (Waza et al., 2005), and heat shock factor 1 (Pratt et al., 2015). It is reasonable to assume that 17AAG may have severe side effects when administered systemically. Fortunately, the antiepileptic activity observed in our study was achieved at concentrations below the maximum tolerated dose that was previously indicated in preclinical safety testing (Musser et al., 2003; Ramanathan et al., 2005). In a clinical study, ∼450 mg/m^2 17AAG was i.v. administered to breast cancer patients (Modi et al., 2011). In our study, 25 mg/kg 17AAG was i.p. injected into mice, which is equivalent to ∼60 mg/m^2 in humans. This dose was effective in inducing GLT1 protein levels because the expression of Hsp90β is relatively low in astrocytes. Although long-term toxicology tests for 17AAG in rodents are still lacking, a previous study showed that mice receiving i.p. injections of 17AAG for 5 mo exhibited neither infertility nor liver or renal dysfunction at a dose of 25 mg/kg (Waza et al., 2005), suggesting that low-dose and prolonged administration of 17AAG or much less toxic Hsp90 inhibitors have the potential for clinical application.

Considering that Hsp90β, but not Hsp90α, is extensively up-regulated in astrocytes during the course of TLE,

specifically inhibiting Hsp90β could have fewer side effects. Unfortunately, only a few Hsp90β-specific inhibitors have been developed to date, and none have been widely investigated at molecular, cellular, and whole-animal levels. Our results suggest an alternative approach to disrupt the interaction between Hsp90β and GLT-1. A protein-truncation assay revealed that the interaction between GLT-1 and Hsp90β requires a specific domain within the region between HP1 and the eighth transmembrane domain. Considering the conformation of GLT-1 at the lipid bilayer (Fig. 4 D; Vandenberg and Ryan, 2013), the inner peptides around HP1 are likely to mediate the interaction between GLT-1 and Hsp90β. This region is constantly exposed to the cytoplasm, regardless of whether GLT-1 is packaged in transport vesicles or located at the cell membrane. It would thus be reasonable to develop a compound that specifically disrupts the interaction between Hsp90β and GLT-1 to inhibit GLT-1 degradation.

We believe our work paves the way for future investigations on the therapeutic potential of Hsp90 inhibitors in TLE and other excitotoxicity-related disorders. Although Hsp90-based therapies may offer a new treatment strategy for refractory epilepsy, the potential side effects and toxicities of 17AAG or new-generation Hsp90 inhibitors must still be addressed. Furthermore, understanding the molecular mechanisms underlying the activation of Hsp90β in reactive astrocytes is also very important for advancing this therapeutic approach.

MATERIALS AND METHODS

Human tissue

Two neuropathologists reviewed all cases. In seven TLE patients, HS without extrahippocampal pathology was identified. In the other five patients, focal lesions, including gliomas, cortical dysplasia, or oligodendroglioma, were observed, but they did not involve the hippocampus proper and histological examination revealed no significant hippocampal neuronal loss in these patients (nonHS). The nonHS subjects were used as a control group for comparison with the HS cases. Autopsy hippocampi were obtained from autopsy of five patients without a history of epilepsy or other neurological diseases. All autopsies were performed within 12 h of death. All patients gave written informed consent and all procedures were undertaken with the approval of the institutional review board of Chinese Academy of Medical Sciences and Peking Union Medical College (CAMS and PUMC; Beijing, China).

Animals

Adult male or newborn C57BL/6J mice (Vital River) were used for this study. All adult animals were housed in cages with littermates and free access to water and food under 12-h light/dark schedules. Mice were handled in accordance with protocols approved by the institutional review board of CAMS and PUMC and were conducted within the terms of the Beijing administration office of laboratory animal guidelines for the care and use of laboratory animals.

Tsc1$^{flox/flox}$;GFAP-Cre conditional knock-out mice (abbreviated as: *Tsc1*^{GFAP} CKO) were generated with the following mice: a floxed mutant mouse possessing loxP sites flanking exons 17 and 18 of the Tsc1 gene (Tsc1^{tm1Djk}/J; The Jackson Laboratory; Tsc1$^{fl/fl}$) and a hemizygote mouse expressing Cre recombinase under the control of the human glial fibrillary acidic protein promoter (FVB-Tg(GFAP-cre)25Mes/J; The Jackson Laboratory; hGFAP-Cre). All mice used for experiments (including control groups) were obtained from our inbred strains. Genomic DNA was isolated from tails of 2–3-wk-old mice by the traditional phenol/chloroform method, and genotyping was performed according to the manufacturers' specifications. Both male and female *Tsc1*^{GFAP} CKO mice were used for the studies in an equal distribution between two groups. Littermate mice were used as control in all animal experiments.

Chemicals

The following chemicals were used at the indicated concentrations: TGFβ (R&D Systems), KA monohydrate (Sigma-Aldrich), ceftriaxone (Sigma-Aldrich), CHX (Sigma-Aldrich), MG132 (Sigma-Aldrich), GA (LC Laboratories), 17AAG (LC Laboratories), VER-155008 (Selleck), and DMSO (Ameresco).

Primary culture of mouse cerebral cortical astrocytes

Primary dissociated astrocyte cultures were prepared as previously described (Miralles et al., 2001). Cerebral cortices of newborn C57BL/6J pups were removed and cleaned of meninges and blood vessels. The remaining tissue was mechanically dissociated with a 25-gauge needle and suspended in DMEM (Macgene) with 10% FBS (Gibco), 100 U/ml penicillin, and 100 mg/ml streptomycin (Macgene). Isolated cells were primary cultured on T75 cm^2 flasks (Falcon) and maintained in a humid atmosphere of CO_2/air (5%/95%) at 37°C for 7–10 d without changing the culture medium. After they reached confluence, microglia and oligodendrocytes were removed by placing the flasks in a heated shaker (37°C) overnight. Astrocytes were then replated onto poly-D-lysine-coated dishes for subsequent experiments.

Acute model of seizures

For the acute seizure study, electrodes and cannulae were implanted before KA injection, as previously described (Sha et al., 2014). After surgery, mice were allowed a 7-d recovery period and were then injected with 5–25 mg/kg 17AAG (dissolved in 50 µl DMSO). The control group received DMSO alone. 24 h after injection, a total of 10 ng of KA in 0.5 µl PBS was injected into the hippocampus through the implanted cannula to induce acute seizures. The number of seizures refers to the total number of seizures after KA application. The time of seizures was measured by adding up the time elapsed from the first to the last seizure event. The onset of seizure was defined by the time elapsed from KA injection to the occurrence of the first EEG seizure. The duration of each seizure was averaged from the duration of every ictal episode.

Post-SE model of epilepsy and vEEG analysis

A KA-induced mouse model of spontaneous seizures was established as previously described (Sha et al., 2012). After unilateral intrahippocampal injection of 200 ng KA, mice experienced at least 2 h of convulsive SE, whereas SRSs and HS (the epileptic foci) developed within 2 wk. At 4–5 wk after KA injection, each animal was implanted with a hippocampal depth electrode. After a 1-wk recovery period, the baseline of motor seizures was recorded for 20–25 consecutive days. The selected mice were then injected i.p. with 17AAG or DMSO (vehicle control) and monitored continuously for 35–45 d for spontaneous seizures by video electroencephalogram (vEEG) recording. An every other day injection protocol was used for DMSO and 17AAG (25 mg/kg in 50 µl of DMSO). For the ceftriaxone study, the mice received a daily injection of ceftriaxone (50 µl, 200 mg/kg, i.p.) according to the experiment schedule, whereas the control group received the vehicle solution alone.

For wired EEG recordings, animals were housed individually in specially constructed cages, each fitted with an amplifier (Andy) and a varifocal IR digital camera (Sony). The vEEG data were reviewed to identify motor seizures by two trained experimenters blinded to the experimental conditions. Each epileptic seizure could be clearly identified by a burst of high amplitude EEG activity with limb clonus or general tonic-clonic seizures. The baseline seizure frequency (number of seizures per day) was measured from all vEEG data recorded during the preinjection baseline. Seizure frequency during drug injection was measured from vEEG data acquired between the day 9 and the endpoint because 17AAG exhibited an anticonvulsant effect after mice received at least four 17AAG injections.

Interictal spikes were identified and defined as fast (<200 ms) epileptiform waveforms that were at least twice the amplitude of the background activity. For the analysis, the sum of interictal spikes of 10 randomly selected 1-min epoch EEG data per day were calculated. Data for the last 5 d during the preinjection baseline and from days 21–25 after 17AAG injection were analyzed and are presented as the interictal spike frequency (number of spikes per 10 min).

Anatomical processing, immunohistochemistry (IHC), and cell quantification procedures

At the endpoint of vEEG monitoring, the mice were euthanized for pathological studies. For IHC staining, the brains were quickly removed and fixed in a 4% paraformaldehyde solution for 24 h at 4°C and then embedded in paraffin. The paraffin-embedded tissues were sectioned at 4 µm and mounted on precoated glass slides. The following primary antibodies were used: anti-GFAP antibody (1:2,000; #AB5541; EMD Millipore); GFAP (D1F4Q) XP rabbit mAb (1:2,000; #12389; CST); iba1 (1:50; ab5076; Abcam); Hsp90α (1:200; ab109248; Abcam); and Hsp90β (1:200; ab32568; Abcam). All photographs were captured with an inverted fluorescence microscope (DMI4000B; Leica).

For the quantitative evaluation of $Hsp90\alpha^+$ or $Hsp90\beta^+$ glia-like cells in human brain tissues, two sections per subject were used. In each experiment, autopsy, nonHS, and HS tissues were simultaneously stained. Cell counting in the human hippocampus was performed by evaluating the CA1 and CA3 regions and the hilus of the DG. Two representative and adjacent nonoverlapping fields of the areas of interest were captured (rectangular frames, 40× magnification, 321 µm × 240 µm) and digitized with an inverted fluorescence microscope (DMI4000B; Leica). The number of glia-like cells stained with Hsp90α or Hsp90β was manually counted from the digital images acquired by the microscope. The data are presented as the average number of cells (40× magnification, 321 µm × 240 µm). Double-labeling immunofluorescence studies were used to confirm the cell type specificity.

For the quantitative evaluation of $Hsp90\beta^+$ astrocytes, GFAP, or Timm's staining, and granule-cell dispersions in the mouse brain, three coronal sections along the anterior–posterior axis representing the anterior (anteroposterior, ∼1.4 mm), medial (anteroposterior, ∼2.0 mm), and posterior (anteroposterior, ∼2.4 mm) regions of the hippocampus were measured. The number of $Hsp90\beta^+$ astrocytes in the mouse models of epilepsy and FS was counted in each region of interest and averaged (DG, CA1, and CA3; 40× magnification, 321 µm× 240 µm). For quantification of GFAP IHC and Timm's staining, the entire hippocampus was captured using a 5× objective lens in each section. Binary images were obtained, and the area occupied by GFAP IHC and Timm's staining within the hippocampus proper was measured using ImageJ software (National Institutes of Helath).

To quantify the granule-cell dispersions, the distances from the inner (hilar) border of the granule cell layer to the outer border of the most distal granule cell somata were determined using previously described procedures (Haas and Frotscher, 2010). The mean and standard deviation of six measurements in three representative sections were calculated for each animal.

Timm's staining

Timm's staining was performed as previously described (Wang et al., 2016). Mice were anesthetized and perfused intracardially with 50 ml 0.9% NaCl (Sigma-Aldrich) solution, followed by 50 ml 4% paraformaldehyde solution (Sigma-Aldrich), 100 ml 1% sodium sulfide solution (Sigma-Aldrich), and 50 ml 4% paraformaldehyde solution again. Slices were stained in Timm's developer solution for 110 min in darkness at room temperature. Timm's developer solution was freshly made from 60 ml gum arabic (30 g; Vetec), 10 ml citric acid monohydrate (2.55 g; Beijing Chemical Works) and trisodium citrate dehydrate (2.35 g; Beijing Chemical Works), 15 ml hydroquinone (0.85 g; Sigma-Aldrich), and 15 ml silver nitrate (0.11 g; Sinopharm Chemical Reagent). Subsequently, sections were washed with distilled water and counterstained with hematoxylin (ZSGB-BIO). An investigator blinded to the treatment assessed the degree of mossy fiber sprouting

into the supragranular layer of the DG. The standard for scoring was described previously (Wang et al., 2016).

Plasmid constructs and transfection

GLT-1-myc, ub-HA (ribosomal protein S27a, RPS27A), GLT-1-FLAG, GLT-1-myc, Hsp90β-myc, and Hsp90β-FLAG were cloned into the pcDNA3.1 vector (V855-20; Invitrogen). The GLT-1 K-to-R gene is synthesized from Tsingke. Deletion mutants were generated by a PCR-based approach. NEOFECT DNA-transfection reagent (Neofect Biotech) was used for transient transfection of plasmids in accordance with the manufacturer's instructions. Hsp90-1 (sc-35610), GLT-1 (sc-35256), and control siRNA were obtained from Santa Cruz Biotechnology, Inc. Hsp90-2 siRNA (5′-GAA GTTCTATGAGGCCTTCTCCAAA-3′) was synthesized from Ribobio. Astrocytes were transfected with siRNA using X-tremeGENE siRNA Transfection reagent (Roche) according to manufacturer's protocol.

Lentivirus packaging

The genes encoding Hsp90α and Hsp90β were subcloned into the pLV-EGFP-N plasmid (Inovogen Tech. Co). 293t cells were cotransfected with the lentiviral vector and the lentiviral packaging/envelope vectors pH1 and pH2 at a molar ratio of 3:3:2. Viruses were collected from the culture supernatant 48 h after transfection and spun at 4,000 rpm for 15 min to remove cell debris. The supernatant was passed through a 0.45-μm filter and lentivirus was purified by ultracentrifugation. Astrocytes were transduced with lentiviral construct for at least 48 h at a multiplicity of infection of 20.

In vivo Hsp90β expression by AAV vector

The AAV expression vector containing AAV2 inverted terminal repeats was used to express Hsp90β under the control of the CMV promoter. The vector was packaged with capsid sequences from AAV2 or AAV5 to produce AAV pseudotypes. AAV2 packaging plasmid pXX2 and Ad help plasmid pXX680 were provided by R.J. Samulski (University of North Carolina, Chapel Hill, NC). AAV5 packaging plasmid pAAV2/5 and pAd DeltaF6 were provided by Penn Vector Core (University of Pennsylvania, Philadelphia, PA). Recombinant AAV vectors were generated by triple transfection of 293t cells at a molar ratio of 1:1:1 using NEOFECT DNA transfection reagent (Neofect biotech) and were purified using the chloroform-PEG8000/NaCl-chloroform method and ultrafiltration. The titers of the obtained viruses were analyzed by real-time PCR. A total amount of 4×10^9 genome copies per 2-μl injection was used. To determine the cell type–specific expression of AAV5-mediated gene transfer in the sclerotic hippocampus, three animals per group were sacrificed for immunofluorescence staining at 1 mo after AAV2-GFAP or AAV5-GFP injection.

Quantitative real-time PCR

Total RNA from astrocyte cultures was extracted using TRIzol (Thermo Fisher Scientific) according to the manufacturer's protocol. The cDNA was prepared using Fast Lane Cell cDNA kit (QIAGEN). Levels of mRNA were assessed by real-time PCR using SYBR supermix (Bio-Rad Laboratories). A fragment of actin was amplified as the internal control. The following forward (F) and reverse (R) primers were used to amplify GLT-1 and actin: GLT-1 (F), 5′-TAGATATGTCGGTTG CCGTTTG-3′, GLT-1 (R), 5′-AGCCCAGTCCACCAG TGAGG-3′; Actin (F), 5′-GAGATTACTGCCCTGGCT CCTA-3′, Actin (R), 5′-TCATCGTACTCCTGCTTGCTG AT-3′. Differences in gene expression were calculated using the ΔΔCT method and are presented as the relative fold change.

Cell lysis and immunoprecipitation

Cells or brain tissues washed once with cold PBS were solubilized or homogenized on ice in Cellytic lysis buffer (C2978; Sigma-Aldrich) supplemented with protease inhibitors (250 mM PMSF, 5 mg/ml pepstatin A, 10 mg/ml leupeptin, and 5 mg/ml aprotinin). Cleared lysates were obtained by centrifugation at 12,000 rpm for 10 min at 4°C, and 0.7–1.2 mg of the lysates were used for immunoprecipitation. Lysates were incubated with primary antibodies overnight at 4°C and incubated for 2 h with a 50% slurry of protein A/G Sepharose. After three rinses with PBS, immunoprecipitated proteins were recovered from the beads by boiling for 10 min in sample buffer or by competition with the tag peptide and then analyzed by immunoblotting. Anti-FLAG mouse mAb (#8146; Cell Signaling Technology), Myc mouse mAb (#2276; Cell Signaling Technology), and anti-Myc agarose (A7470; Sigma-Aldrich) were used against epitope tags. For endogenous coimmunoprecipitation from primary cultured astrocytes, cell lysates were incubated with rabbit anti–GLT-1 antibody (ab178401; Abcam). Anti-EAAT2 antibody (ab205247; Abcam) was used for in vivo coimmunoprecipitation from mouse hippocampal tissues, which were dissected from the hippocampus ipsilateral to KA injection at 5 wk after SE.

Pulse-chase experiment

The pulse-chase experiment was performed according to manufacturer's instructions (EZ-Link Sulfo-NHS-SS-Biotin; Thermo Fisher Scientific). In brief, the cells were washed three times with PBS, and then incubated with 1 mg/ml Sulfo-NHS-SS-Biotin in PBS for 30 min at 37°C, with gentle shaking every 5 min. The cells were then washed three times with quenching buffer (25 mM Tris in PBS) to remove any nonreacted biotinylation reagent. After biotinylation, cells were cultured in DMSO or 17AAG (200 nM) for 12 or 24 h and harvested for assessing biotin-labeled protein by incubation with NeutrAvidin Agarose Resins (Thermo Fisher Scientific) overnight at 4°C. The next day, after three rinses with PBS, the biotin-labeled proteins were recovered from the agarose by boiling for 10 min in sample buffer and were used for Western blot.

Western blot

Protein extraction and Western blot were performed as previously described (Sha et al., 2014). Membrane and cytosolic

proteins were extracted using Mem-PER Plus Membrane Protein Extraction kit (Thermo Fisher Scientific). The following antibodies were used: from Abcam against Hsp90α antibody (1:2,000; ab109248), Hsp90β (1:2,000; ab32568), GLT-1 (1:500; ab178401), glutamine synthetase (GS, 1;2,000; ab64613), and xCT (1;2,000; ab37185); from Cell Signaling Technology against Hsp90β (1:2,000; #5087), Hsp70 (1:2,000; #4873), GFAP (1:2,000; #12389), HA tag (1:2,000; #3724); FLAG Tag (1:2,000; #8146), and Myc Tag (1:2,000; #2276); from Santa Cruz Biotechnology, Inc. against GLT-1 (1:500; sc-15317), Glast antibody (1:500; sc-15316), and 20S Proteasome β1 antibody (1:500; sc-67345); from Sigma-Aldrich against Tubulin (1:20,000; T6557), Actin (1:20,000; A5060), and GAPDH antibody (1:20,000; G9545). Band intensities of treatment groups were normalized to controls and expressed as the fold change.

Proximity ligation assay (PLA) analysis

Duolink In Situ Detection Reagents Green (DUO92014, Sigma-Aldrich), PLA Probe Anti–Rabbit MINUS (DUO92005-100RXN, Sigma-Aldrich) and PLA Probe Anti–Mouse PLUS (DUO92001-100RXN, Sigma-Aldrich) were used in PLA assay according to the manufacturer's instructions. Primary cultured astrocytes grown on coverslips were used for assay. After 17AAG treatment for 48 h, cells were washed twice with PBS, fixed with 4% paraformaldehyde for 10 min, permeabilized with 0.25% Triton X-100 for 10 min at 4°C, incubated with 5% BSA for 1 h to block nonspecific antibody binding, then incubated with primary antibodies overnight at 4°C. The following antibodies were used: anti-EAAT2 antibody (1:125; sc15317; Santa Cruz Biotechnology, Inc.) and anti-Hsp90β antibody (1:1,000; ab53497; Abcam). The next day, the slips were washed twice with wash buffer and incubated with probes for 1 h at 37°C. The slips were then washed twice again, ligated (30 min, 37°C) and amplified (100 min, 37°C). The slides were washed twice with wash buffer, mounted onto slides with DAPI-containing medium (Vector Laboratories) and analyzed by confocal microscopy (LSM510 or LSM700; ZEISS). Amplifier offset and detector gain were adjusted first and never changed in the course of an experimental session. Each discrete green spot represents a GLT-1–Hsp90β protein complex. For each treatment, fluorescent images were obtained from at least eight randomly selected fields under a 20× objective per well and processed by ImageJ software. The total number of dots per image was normalized to the number of DAPI nuclei to obtain the signal-per-cell ratio.

Hippocampal microdialysis

In vivo microdialysis and glutamate concentration assay was performed as previously described (Zeng et al., 2010). AtmosLM system (Eicom) and microdialysis probes (CX-I-3-02; Eicom) were used in this study. Mice were anesthetized with chloral hydrate (500 mg/kg, i.p.) and placed in a stereotaxic frame (Digital Lab Standard Stereotaxic). A guide cannula (CXG-3; Eicom) was stereotactically implanted into the hippocampus ipsilateral to KA injection (anteroposterior = –2.0 mm; mediolateral = –1.8 mm, dorsoventral = –2.3 mm) at 5 wk after SE. 3 wk after the drug injection, a microdialysis probe connected to a syringe pump was attached to the guide cannula, and artificial cerebrospinal fluid (ACSF: 1.3 mM $CaCl_2$, 1.2 mM $MgSO_4$, 3 mM KCl, 0.4 mM KH_2PO_4, 25 mM $NaHCO_3$, and 122 mM NaCl, pH 7.35) was perfused through the microdialysis probe. Microdialysis was performed at flow rates of 1.5, 1.0, 0.8, 0.6, and 0.4 µl/min. First, four 1-h samples were taken at 1.5 µl/min to ensure that ECF glutamate levels reached a steady-state concentration after probe insertion. Then, samples were collected hourly into 0.2-ml Eppendorf tubes for subsequent measurement of glutamate concentrations. Glutamate concentrations from different flow-rate samples were used to calculate the in vivo concentration of glutamate within the brain ECF, which was based on a second-order polynomial equation: $y = (a \times x^2) + (b \times x) + E$ (y = glutamate concentration, x = flow rate, E = extrapolated in vivo ECF concentration at zero flow). The percent recovery of glutamate at each flow rate was determined by the following equation: $(Cx/E) \times 100$ (Cx = glutamate concentration at a given flow rate, E = in vivo concentration calculated by extrapolation). After microdialysis was completed, the mice were sacrificed to allow histological confirmation of the microdialysis probe location in the hippocampus. Dialysate glutamate concentrations were measured using an Amplex red glutamic acid/glutamate oxidase assay kit (Molecular Probes).

Extracellular glutamate clearance

Glutamate clearance was performed as previously described (Wang et al., 2016). 6 h before 17AAG (100 nM; 48 h) treatment was finished, astrocytes cultured in 6-well plates were glutamate depleted for another 12 h in Opti-MEM (Opti-MEM) containing 2% FBS (Gibco). Medium was removed and the plates were washed twice with uptake buffer (1.2 mM KH_2PO_4, 1.3 mM $CaCl_2$, 10 mM D-Glucose, 122 mM NaCl, 3.3 mMKCl, 0.4 mM $MgSO_4$, 25 mM Hepes, pH 7.4, all from Sigma-Aldrich). Then, 2 ml uptake buffer containing glutamate was immediately added to each well. At each time point, 100 µl supernatant was collected and centrifuged for 10 min at 3,500 rpm. Extracellular glutamate concentrations were determined using the Amplex Red Glutamic Acid/Glutamate Oxidase Assay kit (Molecular Probes) and according to the manufacturer's protocol. Data are presented as the decreasing curve of extracellular glutamate concentrations.

^{3}H-Glutamate uptake assay for astrocytes and PMVs

Glutamate uptake was assessed according to a previously published protocol (Frizzo et al., 2002). Treated astrocytes were plated in 24-well plates and washed twice with PBS and then incubated in Kreb's buffer (Na-containing buffer: 135 mM NaCl, 5 mM KCl, 0.6 mM $MgSO_4$, 1 mM $CaCl_2$, 6 mM D-glucose, and 10 mM Hepes, pH 7.5) with

19.6 nM ^{3}H-glutamate (0.5 µCi; specific activity = 50.8 Ci/mmol; PerkinElmer) and 40 µM unlabeled glutamate (Sigma-Aldrich) for 10 min at 37°C.

Glutamate uptake in the PMVs was performed as previously described (Guo et al., 2003). Mouse brain tissues were homogenized in sample buffer (320 mM sucrose in 50 mM Tris-HCl, pH 7.4) using a Dounce homogenizer and then centrifuged at 1,000 *g* for 10 min at 4°C to remove cellular debris. The supernatant was then centrifuged at 20,000 *g* for 30 min at 4°C, and the resultant PMV pellet was resuspended in Krebs buffer. For each assay, 100 µg PMVs protein samples were used. The samples were incubated in 400 µl Krebs buffer, which contained 0.1 µCi [^{3}H]-glutamate and 10 µM unlabeled glutamate, for 4 min at 37°C.

To distinguish DHK-sensitive [^{3}H]-glutamate uptake from DHK-insensitive uptake, cells were incubated with 100–300 µM DHK (Santa Cruz Biotechnology, Inc.) 1 h before the uptake assay. After incubation, buffer was replaced with ice-cold PBS (HyClone) to stop the uptake of glutamate, and the cells were lysed in 0.3 M NaOH for 30 min at 37°C, which was neutralized with 0.3 M HCl. The lysate was analyzed for both [^{3}H]-glutamate using a liquid scintillation counter (LS 6500 scintillation counter; Beckman Coulter) and protein content using Bradford Protein Assay kit (Bio-Rad Laboratories). The radioactivity and the total protein concentration were used to calculate the amount of glutamate (in nanomolars) taken up by the astrocytes per mg of protein over a 10-min period. DHK-sensitive [^{3}H]-glutamate uptake was calculated by subtracting DHK-insensitive Na^{+}-dependent [^{3}H]-glutamate uptake (DHK-treated sample) from total Na^{+}-dependent, ^{3}H-glutamate uptake. All measurements are normalized to the mean glutamate uptake obtained from the control and were performed in triplicate.

Data analysis

Statistical significance was calculated using Prism software (GraphPad), and unpaired two-sided Student's *t* tests or Mann–Whitney *U* tests were used to analyze the significance between two experimental groups. One-way ANOVA followed by Tukey's or Dunnett's tests were used for multiple comparisons. The data are presented as the mean ± SEM unless otherwise noted. All animals were present at the end of the study. No data points were excluded. All histopathological and EEG analyses were performed in a blinded manner.

Online supplemental material

Fig. S1 shows the Hsp90α and Hsp90β staining in the hippocampi of the epilepsy models and patients with TLE. Fig. S2 shows that the Hsp90 inhibitor, but not the Hsp70 inhibitor, increases GLT-1 protein levels. Fig. S3 shows the interaction of GLT-1 and Hsp90β in vivo and in vitro. Fig. S4 shows the effects of 17AAG on seizure frequency, interictal epileptiform discharges, and brain structure. Fig. S5 shows the effects of 17AAG on ECF glutamate levels, GLT-1 expression and histological abnormalities in the sclerotic hippocampus.

ACKNOWLEDGMENTS

We thank Drs. Jun Wei and Fen-biao Gao for their helpful suggestions on this manuscript. We thank Dr. Weimin Tong at PUMC for kindly providing genetic tools and suggestions about animal experiments. We thank Dr. Ye Zhang at PUMC for providing Hsp90 plasmid. We thank Dr. Susan Amara for providing CMV-hEAAT2 plasmid. We thank Dr. David J. Kwiatkowski for providing *Tsc1*$^{flox/flox}$ transgenic mice and Dr. Albee Messing for providing GFAP-cre transgenic mice. We also thank Penn Vector at the University of Pennsylvania for providing the AAV-related plasmids used in this research.

This work was supported by the research grants from the National Basic Research Program of China (2013CB531301), the National Natural Science Foundation of China (81501131, 81471325, 31430048, and 81625008), Beijing Municipal Science and Technology Commission (Z151100003915119), PUMC Youth Fund (3332016134), and CAMS Innovation Fund for Medical Sciences (2016-I2M-1-004).

The authors declare no competing financial interests.

Author contributions: Q. Xu and Y. Shen supervised the whole project. L. Sha conceived the study. L. Sha and X. Wang designed and performed most of the experiments, analyzed the data, and wrote the manuscript. J. Li assisted with some animal experiments. X. Shi participated in some in vitro experiments. L. Wu provided tissue samples and advice on histological experiments. All of the authors read and discussed the manuscript.

Submitted: 8 May 2016
Revised: 11 October 2016
Accepted: 13 December 2016

REFERENCES

Auluck, P.K., M.C. Meulener, and N.M. Bonini. 2005. Mechanisms of suppression of alpha-synuclein neurotoxicity by geldanamycin in *Drosophila*. *J. Biol. Chem.* 280:2873–2878. http://dx.doi.org/10.1074/jbc.M412106200

Bouilleret, V., V. Ridoux, A. Depaulis, C. Marescaux, A. Nehlig, and G. Le Gal La Salle. 1999. Recurrent seizures and hippocampal sclerosis following intrahippocampal kainate injection in adult mice: electroencephalography, histopathology and synaptic reorganization similar to mesial temporal lobe epilepsy. *Neuroscience.* 89:717–729. http://dx.doi.org/10.1016/S0306-4522(98)00401-1

Bristol, L.A., and J.D. Rothstein. 1996. Glutamate transporter gene expression in amyotrophic lateral sclerosis motor cortex. *Ann. Neurol.* 39:676–679. http://dx.doi.org/10.1002/ana.410390519

Chen, B., W.H. Piel, L. Gui, E. Bruford, and A. Monteiro. 2005. The HSP90 family of genes in the human genome: insights into their divergence and evolution. *Genomics.* 86:627–637. http://dx.doi.org/10.1016/j.ygeno.2005.08.012

Cudkowicz, M.E., S. Titus, M. Kearney, H. Yu, A. Sherman, D. Schoenfeld, D. Hayden, A. Shui, B. Brooks, R. Conwit, et al. Ceftriaxone Study Investigators. 2014. Safety and efficacy of ceftriaxone for amyotrophic lateral sclerosis: a multi-stage, randomised, double-blind, placebo-controlled trial. *Lancet Neurol.* 13:1083–1091. http://dx.doi.org/10.1016/S1474-4422(14)70222-4

Dimopoulos, M.A., C.S. Mitsiades, K.C. Anderson, and P.G. Richardson. 2011. Tanespimycin as antitumor therapy. *Clin. Lymphoma Myeloma Leuk.* 11:17–22. http://dx.doi.org/10.3816/CLML.2011.n.002

Dubé, C., C. Richichi, R.A. Bender, G. Chung, B. Litt, and T.Z. Baram. 2006. Temporal lobe epilepsy after experimental prolonged febrile seizures: prospective analysis. *Brain.* 129:911–922. http://dx.doi.org/10.1093/brain/awl018

Egorin, M.J., E.G. Zuhowski, D.M. Rosen, D.L. Sentz, J.M. Covey, and J.L. Eiseman. 2001. Plasma pharmacokinetics and tissue distribution of 17-(allylamino)-17-demethoxygeldanamycin (NSC 330507) in CD2F1 mice1. *Cancer Chemother. Pharmacol.* 47:291–302. http://dx.doi.org/10.1007/s002800000242

Eleuteri, A.M., M. Cuccioloni, J. Bellesi, G. Lupidi, E. Fioretti, and M. Angeletti. 2002. Interaction of Hsp90 with 20S proteasome: thermodynamic and kinetic characterization. *Proteins.* 48:169–177. http://dx.doi.org/10.1002/prot.10101

Frizzo, M.E.D., D.R. Lara, A.S. Prokopiuk, C.R. Vargas, C.G. Salbego, M. Wajner, and D.O. Souza. 2002. Guanosine enhances glutamate uptake in brain cortical slices at normal and excitotoxic conditions. *Cell. Mol. Neurobiol.* 22:353–363. http://dx.doi.org/10.1023/A:1020728203682

Fujikake, N., Y. Nagai, H.A. Popiel, Y. Okamoto, M. Yamaguchi, and T. Toda. 2008. Heat shock transcription factor 1-activating compounds suppress polyglutamine-induced neurodegeneration through induction of multiple molecular chaperones. *J. Biol. Chem.* 283:26188–26197. http://dx.doi.org/10.1074/jbc.M710521200

García-Tardón, N., I.M. González-González, J. Martínez-Villarreal, E. Fernández-Sánchez, C. Giménez, and F. Zafra. 2012. Protein kinase C (PKC)-promoted endocytosis of glutamate transporter GLT-1 requires ubiquitin ligase Nedd4-2-dependent ubiquitination but not phosphorylation. *J. Biol. Chem.* 287:19177–19187. http://dx.doi.org/10.1074/jbc.M112.355909

Guo, H., L. Lai, M.E.R. Butchbach, M.P. Stockinger, X. Shan, G.A. Bishop, and C.L.G. Lin. 2003. Increased expression of the glial glutamate transporter EAAT2 modulates excitotoxicity and delays the onset but not the outcome of ALS in mice. *Hum. Mol. Genet.* 12:2519–2532. http://dx.doi.org/10.1093/hmg/ddg267

Haas, C.A., and M. Frotscher. 2010. Reelin deficiency causes granule cell dispersion in epilepsy. *Exp. Brain Res.* 200:141–149. http://dx.doi.org/10.1007/s00221-009-1948-5

Harvey, A.S., J.D. Grattan-Smith, P.M. Desmond, C.W. Chow, and S.F. Berkovic. 1995. Febrile seizures and hippocampal sclerosis: frequent and related findings in intractable temporal lobe epilepsy of childhood. *Pediatr. Neurol.* 12:201–206. http://dx.doi.org/10.1016/0887-8994(95)00022-8

Héja, L. 2014. Astrocytic target mechanisms in epilepsy. *Curr. Med. Chem.* 21:755–763. http://dx.doi.org/10.2174/09298673206613119160445

Jhaveri, K., T. Taldone, S. Modi, and G. Chiosis. 2012. Advances in the clinical development of heat shock protein 90 (Hsp90) inhibitors in cancers. *Biochim. Biophys. Acta.* 1823:742–755. http://dx.doi.org/10.1016/j.bbamcr.2011.10.008

Kandratavicius, L., J.E. Hallak, C.G. Carlotti Jr., J.A. Assirati Jr., and J.P. Leite. 2014. Hippocampal expression of heat shock proteins in mesial temporal lobe epilepsy with psychiatric comorbidities and their relation to seizure outcome. *Epilepsia.* 55:1834–1843. http://dx.doi.org/10.1111/epi.12787

Kong, Q., K. Takahashi, D. Schulte, N. Stouffer, Y. Lin, and C.L. Lin. 2012. Increased glial glutamate transporter EAAT2 expression reduces epileptogenic processes following pilocarpine-induced status epilepticus. *Neurobiol. Dis.* 47:145–154. http://dx.doi.org/10.1016/j.nbd.2012.03.032

Kong, Q., L.C. Chang, K. Takahashi, Q. Liu, D.A. Schulte, L. Lai, B. Ibabao, Y. Lin, N. Stouffer, C. Das Mukhopadhyay, et al. 2014. Small-molecule activator of glutamate transporter EAAT2 translation provides neuroprotection. *J. Clin. Invest.* 124:1255–1267. http://dx.doi.org/10.1172/JCI66163

Kwan, P., S.C. Schachter, and M.J. Brodie. 2011. Drug-resistant epilepsy. *N. Engl. J. Med.* 365:919–926. http://dx.doi.org/10.1056/NEJMra1004418

Li, S., M. Mallory, M. Alford, S. Tanaka, and E. Masliah. 1997. Glutamate transporter alterations in Alzheimer disease are possibly associated with abnormal APP expression. *J. Neuropathol. Exp. Neurol.* 56:901–911. http://dx.doi.org/10.1097/00005072-199708000-00008

Lin, C.L., Q. Kong, G.D. Cuny, and M.A. Glicksman. 2012. Glutamate transporter EAAT2: a new target for the treatment of neurodegenerative diseases. *Future Med. Chem.* 4:1689–1700. http://dx.doi.org/10.4155/fmc.12.122

Luo, W., W. Sun, T. Taldone, A. Rodina, and G. Chiosis. 2010. Heat shock protein 90 in neurodegenerative diseases. *Mol. Neurodegener.* 5:24. http://dx.doi.org/10.1186/1750-1326-5-24

Macaluso, A., M. Bernabucci, A. Trabucco, L. Ciolli, F. Troisi, R. Baldini, R. Gradini, G. Battaglia, F. Nicoletti, and S. Collini. 2013. Analgesic effect of a single preoperative dose of the antibiotic ceftriaxone in humans. *J. Pain.* 14:604–612. http://dx.doi.org/10.1016/j.jpain.2013.01.774

Maroso, M., S. Balosso, T. Ravizza, J. Liu, E. Aronica, A.M. Iyer, C. Rossetti, M. Molteni, M. Casalgrandi, A.A. Manfredi, et al. 2010. Toll-like receptor 4 and high-mobility group box-1 are involved in ictogenesis and can be targeted to reduce seizures. *Nat. Med.* 16:413–419. http://dx.doi.org/10.1038/nm.2127

Miralles, V.J., I. Martínez-López, R. Zaragozá, E. Borrás, C. García, F.V. Pallardó, and J.R. Viña. 2001. Na+ dependent glutamate transporters (EAAT1, EAAT2, and EAAT3) in primary astrocyte cultures: effect of oxidative stress. *Brain Res.* 922:21–29. http://dx.doi.org/10.1016/S0006-8993(01)03124-9

Miyata, Y. 2005. Hsp90 inhibitor geldanamycin and its derivatives as novel cancer chemotherapeutic agents. *Curr. Pharm. Des.* 11:1131–1138. http://dx.doi.org/10.2174/1381612053507585

Modi, S., A. Stopeck, H. Linden, D. Solit, S. Chandarlapaty, N. Rosen, G. D'Andrea, M. Dickler, M.E. Moynahan, S. Sugarman, et al. 2011. HSP90 inhibition is effective in breast cancer: a phase II trial of tanespimycin (17-AAG) plus trastuzumab in patients with HER2-positive metastatic breast cancer progressing on trastuzumab. *Clin. Cancer Res.* 17:5132–5139. http://dx.doi.org/10.1158/1078-0432.CCR-11-0072

Musser, S.M., M.J. Egorin, E.G. Zuhowski, D.R. Hamburger, R.A. Parise, J.M. Covey, K.D. White, and J.L. Eiseman. 2003. Biliary excretion of 17-(allylamino)-17-demethoxygeldanamycin (NSC 330507) and metabolites by Fischer 344 rats. *Cancer Chemother. Pharmacol.* 52:139–146. http://dx.doi.org/10.1007/s00280-003-0630-z

Pratt, W.B., J.E. Gestwicki, Y. Osawa, and A.P. Lieberman. 2015. Targeting Hsp90/Hsp70-based protein quality control for treatment of adult onset neurodegenerative diseases. *Annu. Rev. Pharmacol. Toxicol.* 55:353–371. http://dx.doi.org/10.1146/annurev-pharmtox-010814-124332

Proper, E.A., G. Hoogland, S.M. Kappen, G.H. Jansen, M.G. Rensen, L.H. Schrama, C.W. van Veelen, P.C. van Rijen, O. van Nieuwenhuizen, W.H. Gispen, and P.N. de Graan. 2002. Distribution of glutamate transporters in the hippocampus of patients with pharmaco-resistant temporal lobe epilepsy. *Brain.* 125:32–43. http://dx.doi.org/10.1093/brain/awf001

Ramanathan, R.K., D.L. Trump, J.L. Eiseman, C.P. Belani, S.S. Agarwala, E.G. Zuhowski, J. Lan, D.M. Potter, S.P. Ivy, S. Ramalingam, et al. 2005. Phase I pharmacokinetic-pharmacodynamic study of 17-(allylamino)-17-demethoxygeldanamycin (17AAG, NSC 330507), a novel inhibitor of heat shock protein 90, in patients with refractory advanced cancers. *Clin. Cancer Res.* 11:3385–3391. http://dx.doi.org/10.1158/1078-0432.CCR-04-2322

Rattka, M., C. Brandt, and W. Löscher. 2013. The intrahippocampal kainate model of temporal lobe epilepsy revisited: epileptogenesis, behavioral and cognitive alterations, pharmacological response, and hippoccampal damage in epileptic rats. *Epilepsy Res.* 103:135–152. http://dx.doi.org/10.1016/j.eplepsyres.2012.09.015

Robel, S., S.C. Buckingham, J.L. Boni, S.L. Campbell, N.C. Danbolt, T. Riedemann, B. Sutor, and H. Sontheimer. 2015. Reactive astrogliosis causes the development of spontaneous seizures. *J. Neurosci.* 35:3330–3345. http://dx.doi.org/10.1523/JNEUROSCI.1574-14.2015

Rothstein, J.D., M. Van Kammen, A.I. Levey, L.J. Martin, and R.W. Kuncl. 1995. Selective loss of glial glutamate transporter GLT-1 in amyotrophic lateral sclerosis. *Ann. Neurol.* 38:73–84. http://dx.doi.org/10.1002/ana.410380114

Rothstein, J.D., S. Patel, M.R. Regan, C. Haenggeli, Y.H. Huang, D.E. Bergles, L. Jin, M. Dykes Hoberg, S. Vidensky, D.S. Chung, et al. 2005. Beta-lactam

antibiotics offer neuroprotection by increasing glutamate transporter expression. *Nature.* 433:73–77. http://dx.doi.org/10.1038/nature03180

Sha, L.Z., X.L. Xing, D. Zhang, Y. Yao, W.C. Dou, L.R. Jin, L.W. Wu, and Q. Xu. 2012. Mapping the spatio-temporal pattern of the mammalian target of rapamycin (mTOR) activation in temporal lobe epilepsy. *PLoS One.* 7:e39152. http://dx.doi.org/10.1371/journal.pone.0039152

Sha, L., X. Wu, Y. Yao, B. Wen, J. Feng, Z. Sha, X. Wang, X. Xing, W. Dou, L. Jin, et al. 2014. Notch signaling activation promotes seizure activity in temporal lobe epilepsy. *Mol. Neurobiol.* 49:633–644. http://dx.doi.org/10.1007/s12035-013-8545-0

Susarla, B.T., and M.B. Robinson. 2008. Internalization and degradation of the glutamate transporter GLT-1 in response to phorbol ester. *Neurochem. Int.* 52:709–722. http://dx.doi.org/10.1016/j.neuint.2007.08.020

Takahashi, K., Q. Kong, Y. Lin, N. Stouffer, D.A. Schulte, L. Lai, Q. Liu, L.C. Chang, S. Dominguez, X. Xing, et al. 2015. Restored glial glutamate transporter EAAT2 function as a potential therapeutic approach for Alzheimer's disease. *J. Exp. Med.* 212:319–332. http://dx.doi.org/10.1084/jem.20140413

Tanaka, K., K. Watase, T. Manabe, K. Yamada, M. Watanabe, K. Takahashi, H. Iwama, T. Nishikawa, N. Ichihara, T. Kikuchi, et al. 1997. Epilepsy and exacerbation of brain injury in mice lacking the glutamate transporter GLT-1. *Science.* 276:1699–1702. http://dx.doi.org/10.1126/science.276.5319.1699

Uhlmann, E.J., M. Wong, R.L. Baldwin, M.L. Bajenaru, H. Onda, D.J. Kwiatkowski, K. Yamada, and D.H. Gutmann. 2002. Astrocyte-specific TSC1 conditional knockout mice exhibit abnormal neuronal organization and seizures. *Ann. Neurol.* 52:285–296. http://dx.doi.org/10.1002/ana.10283

Vandenberg, R.J., and R.M. Ryan. 2013. Mechanisms of glutamate transport. *Physiol. Rev.* 93:1621–1657. http://dx.doi.org/10.1152/physrev.00007.2013

Wang, X., L. Sha, N. Sun, Y. Shen, and Q. Xu. 2016. Deletion of mTOR in reactive astrocytes suppresses chronic seizures in a mouse model of temporal lobe epilepsy. *Mol. Neurobiol.*

Waza, M., H. Adachi, M. Katsuno, M. Minamiyama, C. Sang, F. Tanaka, A. Inukai, M. Doyu, and G. Sobue. 2005. 17-AAG, an Hsp90 inhibitor, ameliorates polyglutamine-mediated motor neuron degeneration. *Nat. Med.* 11:1088–1095. http://dx.doi.org/10.1038/nm1298

Weinberg, M.S., B.L. Blake, R.J. Samulski, and T.J. McCown. 2011. The influence of epileptic neuropathology and prior peripheral immunity on CNS transduction by rAAV2 and rAAV5. *Gene Ther.* 18:961–968. http://dx.doi.org/10.1038/gt.2011.49

Whitesell, L., and S.L. Lindquist. 2005. HSP90 and the chaperoning of cancer. *Nat. Rev. Cancer.* 5:761–772. http://dx.doi.org/10.1038/nrc1716

Yu, P., H. Wang, Y. Katagiri, and H.M. Geller. 2012. An in vitro model of reactive astrogliosis and its effect on neuronal growth. *Methods Mol. Biol.* 814:327–340. http://dx.doi.org/10.1007/978-1-61779-452-0_21

Zeng, L.H., A.W. Bero, B. Zhang, D.M. Holtzman, and M. Wong. 2010. Modulation of astrocyte glutamate transporters decreases seizures in a mouse model of Tuberous Sclerosis Complex. *Neurobiol. Dis.* 37:764–771. http://dx.doi.org/10.1016/j.nbd.2009.12.020